ChemComm

ROYAL SOCIETY OF CHEMISTRY

FEATURE ARTICLE

View Article Online
View Journal | View Issue

Cite this: *Chem. Commun.*, 2021, **57**, 1715

Single component photoresponsive fluorescent organic nanoparticles: a smart platform for improved biomedical and agrochemical applications

Amrita Chaudhuri, Amrita Paul, Antara Sikder and N. D. Pradeep Singh *

Received 29th October 2020,
Accepted 8th January 2021

DOI: 10.1039/d0cc07183h

rsc.li/chemcomm

In the last two decades, light responsive nano drug delivery systems (DDSs) have gained considerable importance, particularly in the area of biology and medicine. In general, light responsive nano DDSs are bicomponent and constructed using two ingredients, namely a nanocarrier and a phototrigger. The synthesis of these bicomponent nano DDSs requires multiple steps, which limits their applications. Hence, we have reported single component light responsive nano DDSs using fluorescent organic nanoparticles (FONPs) which acted both as a nanocarrier and a phototrigger. This feature article provides an overview of recently developed light responsive single component FONPs and their applications in the regulated release of anticancer drugs, gasotransmitters, antibacterial agents, and pesticides, and also as efficient PDT agents. We have summarised the synthesis, characterisation, and photophysical, photochemical, and *in vitro* behaviours of these light responsive FONPs. In addition, we also discussed the advantages of using FONPs as a nano DDS for cellular studies like: excellent biocompatibility, efficient cellular internalisation, real time monitoring of the drug release ability inside the cells, and enhanced cytotoxicity due to regulated release of bioactive molecules inside the cells.

Introduction

Photoresponsive nanocarriers have emerged as a promising tool for targeted therapy, as they can regulate the release of caged bioactive molecules in a spatio-temporal fashion using

Department of Chemistry, Indian Institute of Technology Kharagpur, 721302 Kharagpur, West Bengal, India. E-mail: ndpradeep@chem.iitkgp.ac.in

Amrita Chaudhuri

Amrita Chaudhuri received her bachelor's degree in Chemistry Honours (2013) and master's degree in Chemistry (specialization in Organic Chemistry, 2015) from the Vidyasagar University, Midnapore, India. In July 2015, she joined as a PhD student in organic photochemistry under the supervision of Prof. N. D. Pradeep Singh in the department of chemistry, IIT Kharagpur, India. Her current research interests include design, synthesis and photochemical studies of new photoremovable protecting groups, and photoresponsive gasotrasmitter donors and development of light-responsive therapeutic systems.

Amrita Paul

Amrita Paul completed her bachelor's degree in Chemistry in the year 2011 and then achieved her master's degree in Chemistry with specialization in Organic Chemistry in 2013 from the Vidyasagar University, Midnapore, India. In 2020, August, she achieved her PhD degree in organic photochemistry under the supervision of Prof. N. D. Pradeep Singh in the Department of Chemistry, IIT Kharagpur, India. Her research interests involve development of new strategies for the light-triggered release of caged active molecules and synthesis of new photoremovable protecting groups in order to produce efficient delivery systems for biological applications.

non-invasive light as an external stimulus.[1] Their distinctive features, such as smaller size, higher surface area to volume ratio, and better ability to penetrate deeper into tissue, have helped to improve the pharmacokinetics and biodistribution of several chemotherapeutic agents.[2–5] The essential characteristics that a photoresponsive nanocarrier requires for its application in the area of drug and biomolecule delivery are (i) biocompatibility and easy functionalizability, (ii) high caging efficiency and no premature degradation of delivery agents, (iii) being soluble or colloidal in aqueous medium in order to increase the effectiveness of the delivery agents in the biological medium, (iv) extended circulatory half-life and long shelf life, (v) high biodegradability to reduce undesirable side effects, and (vi) the ability to regulate the release of caged bioactive molecules at the target site.[6,7]

In general, photoresponsive nanocarriers can be classified into two main categories: organic nanocarriers (polymers, dendrimers, liposomes and DNA scaffolds) and inorganic nanocarriers (metal oxides, quantum dots, nanotubes, and semiconducting nanocrystals).[8–10] In both types of photoresponsive nanocarriers the active biomolecules are loaded by two strategies: (i) physical entrapment by the nanocarrier or (ii) attachment to the nanocarrier through covalent bonding. In the case of physical entrapment, the active molecules are trapped in the porous channel or container of the nanoparticles, and the pores of these nanoparticles are closed or sealed with a phototrigger (phototriggers are small organic chromophores that initiate the release of active molecules on irradiation with light).[11–15] With covalent anchoring, the active molecules are covalently attached directly to the phototrigger, which is then connected to the nanocarrier.[16–19] In both cases, the activity of the caged active molecule is temporarily switched off. During photolysis, the active molecule gets released from the phototrigger or removed from the porous system by opening the light-activated gate.

The photoresponsive nanocarriers synthesized by the above discussed strategies are generally bicomponent systems; they require two ingredients for their construction, namely a nanoparticle and a phototrigger. They need three crucial steps for their synthesis, which are (i) synthesis of a biocompatible nanocarrier, (ii) surface functionalization of the nanocarrier, and (iii) attachment of the phototrigger to the nanocarrier.[20–22] To overcome the aforementioned synthetic steps for the construction of photoresponsive nanocarriers, which limited their scope of applications, we introduced for the first time single-component photoresponsive organic nanocarriers in which the nanoparticle-sized fluorescent phototrigger itself acts as a nanocarrier for the delivery of bioactive molecules. For the fabrication of these phototriggers as light responsive fluorescent organic nanoparticles (FONPs), we adapted the effective ''reprecipitation technique''.[23,24]

This feature article is mainly focused on the design and development of single component photoresponsive fluorescent organic nanoparticles (FONPs) as drug delivery systems (DDSs) for the regulated release of anticancer drugs, antibacterial agents, gasotransmitters, and agrochemicals. In addition, we also developed single component FONPs as photosensitizers for efficient PDT in cancer treatment (Fig. 1).

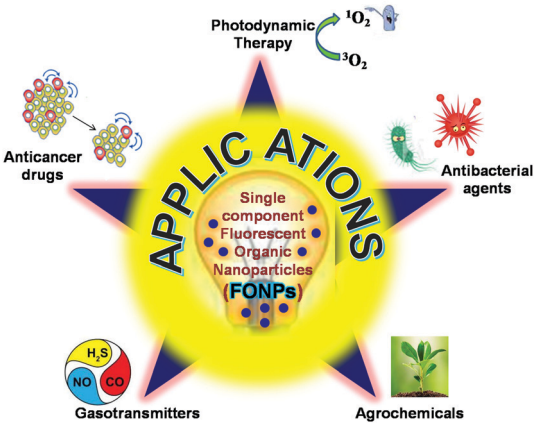

Fig. 1 Single component photoresponsive FONPs for the regulated release of anticancer drugs, antibacterial agents, gasotransmitters, and agrochemicals and as effective PDT agents.

Antara Sikder

Antara Sikder obtained bachelor's degree in Chemistry in the year 2014 from Calcutta University, Kolkata, India, and master's degree in chemistry from IIEST Shibpur, Howrah, India, in 2016. She is currently a PhD student in organic chemistry under the supervision of Prof. N. D. Pradeep Singh in the department of chemistry, IIT Kharagpur, India. Her current research interests involve the design, synthesis and photochemical studies of new photolabile protecting groups and synthesis of light-responsive probes for applications in therapy and diagnostics.

N. D. Pradeep Singh

N. D. Pradeep Singh obtained his BSc and MSc Degrees in Chemistry from University of Madras, Chennai, and conducted research with Prof. A. Anandhan. He completed his PhD study in 2001 at the same institute with Prof. Geetha Gopalakrishnan in Organic Photochemistry. Currently, he is a Professor of Chemistry at the Indian Institute of Technology, Kharagpur, India, and received numerous awards. The Pradeep lab is engaged in the synthesis of new fluorescent photoremovable protecting groups for biological applications and studying visible-light-induced photoredox catalysis.

1 Single component photoresponsive fluorescent organic nanoparticles as a drug delivery system for cancer treatment

1.1 Single component photoresponsive fluorescent organic nanoparticles for regulated release of anticancer drugs

The phototrigger is an important ingredient used in the construction of light responsive drug delivery systems (DDSs). The phototrigger is an organic chromophore which cages the drug molecule in such a way that the activity of the drug molecule is temporarily masked and on exposure to light releases the drug molecule in a controlled manner.[25] In accordance, we also developed several visible light and two-photon activated fluorescent phototriggers based on perylen-3-yl methyl,[26] acetyl pyrene,[27] acridine-9-ylmethyl,[28] carbazole,[29,30] bimane,[31] stilbene,[32] rhodamine,[33] naphthalene,[34] and carboline[35] derivatives for the release of important bioactive molecules. Though phototriggers provide immense scope to control drug release at a specific time and space, thereby providing localised treatment, they also face certain limitations like low solubility in the physiological medium, a lack of targeting ability, and low drug imposing capacity. In order to overcome the limitations of phototriggers and use them efficiently as a DDS, we introduced the strategy of converting these phototriggers to single-component photoresponsive FONPs. Herein, the phototriggers were directly converted into organic nanoparticles by a simple reprecipitation technique, which made them capable of serving both as a nanocarrier and a delivery agent. Photoresponsive organic nanoparticle based DDSs were designed utilising fluorescent phototriggers, and therefore they provided the added advantage of image-guided delivery of drug molecules and the opportunity to monitor the drug release in real-time. In this section, we will illustrate our efforts in designing light-responsive single-component FONPs as anticancer DDSs which were synthesised using phototriggers developed by our group *viz.*, perylene-3-yl methyl,[36] acridin-9-methyl,[37] and *p*-hydroxyphenacyl[38–40] (Fig. 2).

1.1.1 Perylene-3-ylmethanol: single-component photoresponsive fluorescent organic nanoparticles with real-time monitoring of anticancer drug release. In the year 2012, our group for the first time showed the application of single-component FONPs based on perylene-3-ylmethyl for the *in vitro* release of the anticancer drug chlorambucil (Cbl) (Fig. 3A).[36] Photoresponsive organic NPs fabricated using the phototrigger (perylene-3-ylmethanol) exhibited three important features: (i) efficient photorelease in aqueous physiological medium, (ii) a highly fluorescent nature, which helped in image-guided release of drug molecules, and (iii) a distinct fluorescence colour change (red to blue) upon photorelease, which aided in monitoring and quantifying the drug release in real-time.

Nanoparticles of perylene–chlorambucil, Pe–Cbl (DDS), were prepared by the reprecipitation technique, which were globular in shape with an average particle size of ~30 nm (Fig. 3B). Interestingly, the absorption and emission spectra of Pe–Cbl NPs and perylene-3-ylmethanol NPs (phototrigger) were found to be quite different (Fig. 3Ci and ii), which was attributed to the difference in their particle size *i.e.*, 30 nm and 20 nm, respectively. The Pe–Cbl NPs were well dispersed in aqueous medium due to their nano size and hence showed efficient photorelease ability in aqueous physiological medium (Fig. 3D), with about 95% drug release after 30 min of irradiation. On the other hand, the Pe–Cbl conjugate was not able to efficiently photorelease the anticancer drug in aqueous medium due to its insolubility in water. Another fascinating property of Pe–Cbl NPs was that they showed a distinct fluorescence colour change from red (625 nm) to blue (445 nm) upon photolysis. This noticeable blue shift in the emission spectra after the photolysis was due to the difference in the sizes of Pe–Cbl NPs and the photoproduct, perylene-3-ylmethanol NPs. The fluorescence colour change during the photorelease was exploited to monitor and quantify the drug release in real-time. However, the photocaged Pe–Cbl conjugates failed to exhibit the ability of real-time monitoring of drug release.

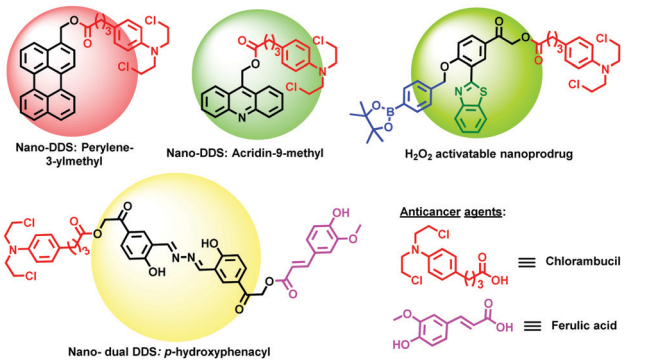

Fig. 2 Single-component photoresponsive fluorescent organic nanoparticles based on perylene-3-yl methyl, acridin-9-methyl, and *p*-hydroxyphenacyl as drug delivery systems for cancer treatment.

In vitro studies revealed that our DDS, Pe–Cbl NPs, showed excellent cellular uptake and good biocompatibility. We also explored the unique real-time monitoring ability of Pe–Cbl NPs for the quantification of the drug release inside HeLa cells using the fluorescence imaging technique (Fig. 3E). The MTT [MTT = 3-(4,5-dimethylthiazol-2-yl)-2,5-diphenyltetrazolium bromide, a yellow tetrazole] assay revealed that Pe–Cbl NPs showed enhanced cytotoxicity compared to free chlorambucil due to precise drug release upon irradiation causing the killing of the cancer cells (Fig. 3F). Hence, we have clearly demonstrated that the nanoparticles of photocaged perylene–chlorambucil seem to be an effective anticancer DDS in comparison to Pe–Cbl conjugates.

1.1.2 Acridin-9-methanol: single component photoresponsive fluorescent organic nanoparticles for nuclear-targeted drug delivery. Though the Pe–Cbl NPs showed excellent properties as a DDS, still they face certain limitations which need to be addressed. One of the main limitations is that the Pe–Cbl NPs were found to be localised mainly in the cellular membrane or in the cytoplasm. It has been well studied that anticancer drugs which work based on a DNA alkylating mechanism need to be delivered into the cell nucleus, in order to efficiently damage

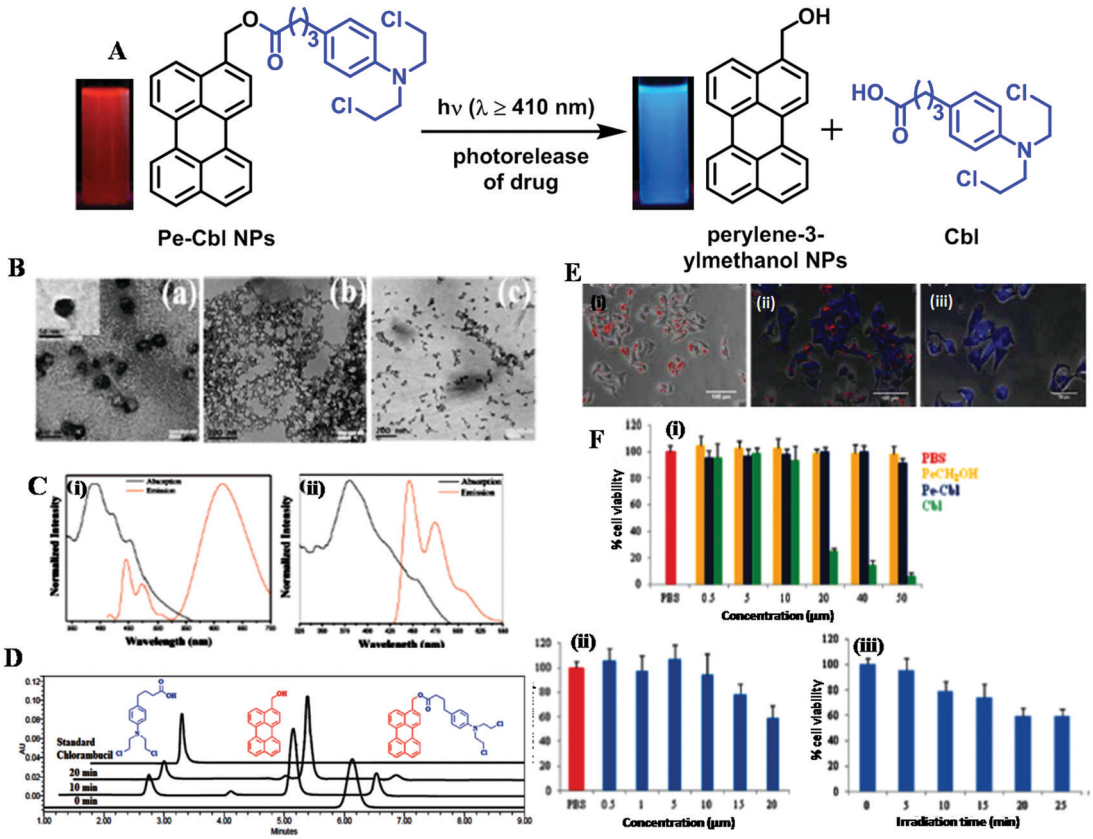

Fig. 3 (A) Schematic representation of photoinduced *in vitro* anticancer drug release from Pe–Cbl NPs with real time monitoring. (B) TEM images of (a) Pe–Cbl NPs before photolysis, (b) Pe–Cbl NPs after photolysis, and (c) perylene-3-ylmethanol NPs. (C) Normalized absorption and emission spectra of (i) Pe–Cbl NPs and (ii) perylene-3-ylmethanol nanoparticles. (D) HPLC profile of Pe–Cbl NPs at regular time intervals of photolysis under visible-light irradiation (≥410 nm). The vertical axes were offset by 15 mAU units and the horizontal axes by 15 s to facilitate better visualization. (E) Real-time drug release studies using confocal microscopy. Shown are overlays of the bright-field image and the fluorescence images in the 445 and 625 nm emission channels (i) before photolysis, (ii) after 10 min of photolysis, and (iii) after 20 min of photolysis. (F) Cell viability tests of Pe–Cbl NPs, perylene-3-ylmethanol nanoparticles, and chlorambucil on the HeLa cell line: (i) before irradiation, (ii) after irradiation in the presence of different concentrations of Pe–Cbl NPs, and (iii) after regular time intervals of irradiation in the presence of 2×10^{-5} M Pe–Cbl NPs. Values are presented as means ± standard deviations. (B–F) are reprinted with permission from ref. 36. Copyright 2012: American Chemical Society.

the DNA and cause cell death. Based on this idea, in the year 2013, we fabricated new single-component fluorescent organic nanoparticles which have high affinity to DNA based on an acridine phototrigger for nuclear-targeted and regulated delivery of anticancer drug chlorambucil (Cbl).[37] The acridin-9-methyl based FONPs performed three important roles: as a (i) ''nuclear-targeted nanocarrier'' for drug delivery, (ii) ''phototrigger'' for regulated drug release, and (iii) fluorescent chromophore for cell imaging (Fig. 4A).

Acridine–chlorambucil (Acr–Cbl) NPs (DDS) and acridin-9-methanol NPs (phototrigger) were found to be spherical in shape with an average particle size of 60 nm (Fig. 4Ba–d). The Acr–Cbl NPs and acridin-9-methanol NPs exhibited quite different absorption spectra; however, their emission spectra were found to be similar, showing a strong blue emission band at 480 nm. Similar to Pe–Cbl nanoparticles, Acr–Cbl NPs were also well dispersed in aqueous medium and showed efficient photorelease ability in aqueous physiological medium under soft visible light irradiation (≥410 nm), with about 90% drug release after 35 min of irradiation. The nuclear targeting ability of the Acr–Cbl NPs was studied using ethidium bromide (EB) displacement assay and docking analysis. The docking analysis revealed that the acridine moiety acted as a minor groove binder (Fig. 4Ci and ii), whereas the ester carbonyl group formed hydrogen bonds with two guanine N7–H atoms. Ethidium bromide displacement assay (Fig. 4Di) revealed that the Acr–Cbl NPs preferred to bind DNA in an intercalative manner. Interestingly, the affinity constant of the Acr–Cbl NPs was found to be 1.59×10^6 M^{-1}, which was similar to that of other strong acridine DNA binders (Fig. 4Dii). Real-time cellular uptake and imaging studies of Acr–Cbl NPs were carried out using the cancerous HeLa cell line. The nuclear colocalization of the Acr–Cbl NPs was compared with the Acr–Cbl conjugate using propidium iodide; the results revealed that the Acr–Cbl NPs showed profound accumulation in the cell nucleus compared to the Acr–Cbl conjugate (Fig. 4E). MTT assay results strongly supported the argument that nuclear targeted delivery of chlorambucil (an alkylating anticancer agent) using Acr–Cbl NPs in regulated release resulted in enhanced anticancer activity.

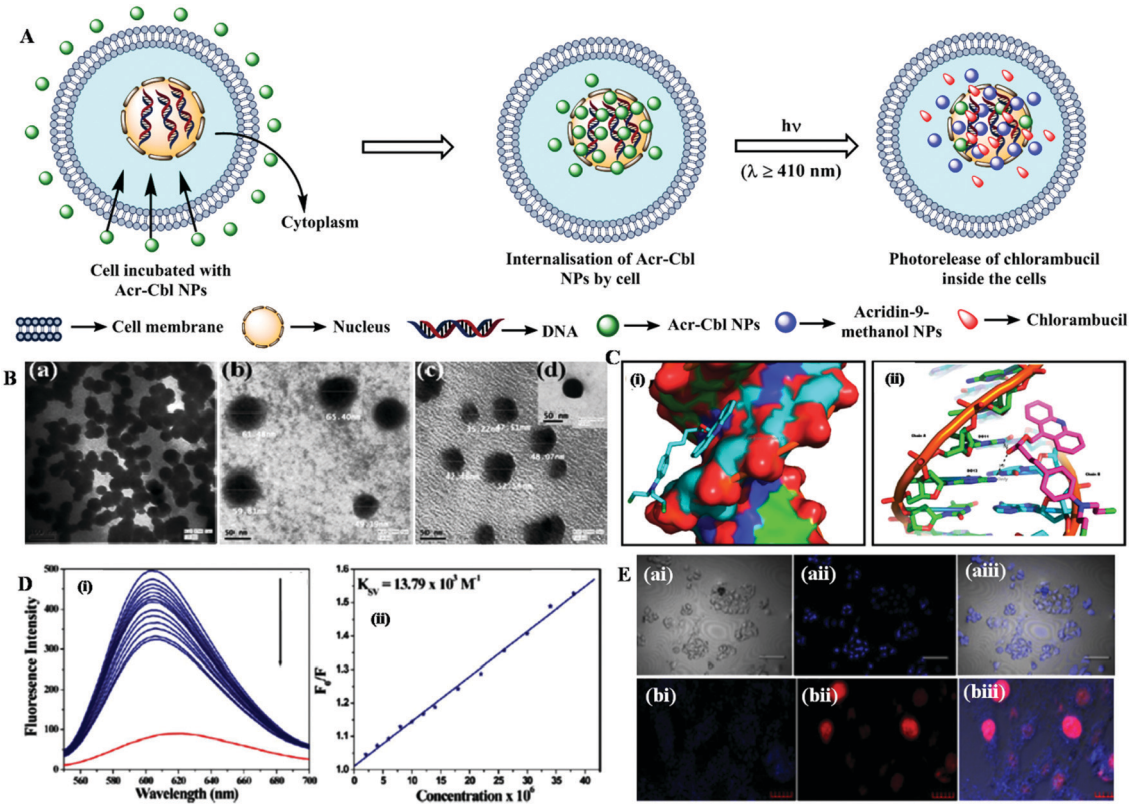

Fig. 4 (A) Schematic presentation of photocontrolled nuclear-targeted delivery of chlorambucil by photoresponsive organic nanoparticles of Acr–Cbl. (B) TEM images of (a and b) Acr–Cbl nanoparticles before photolysis, and (c) Acr–Cbl nanoparticles after photolysis, and (d) TEM image of acridin-9-methanol nanoparticles. (C) Docked conformations of the DNA–Acr–Cbl caged conjugate (i) surface representation showing the binding pockets of the conjugate, and (ii) stereoview of the docked conformations of the Acr–Cbl conjugate showing that the ester carbonyl is forming H-bonds with guanine N_7 H-atoms, thereby facilitating DNA-alkylation. (D) (i) Fluorescence quenching spectra of EB-ct-DNA with Acr–Cbl nanoparticles. The red line indicates the fluorescence emission spectrum of EB in the absence of ct-DNA and the top blue lines indicate the fluorescence emission spectra of EB bound to ct-DNA; [EB] = 2 μM, [ct-DNA] = 20 μM, [Acr–Cbl nanoparticles] = 0–38 μM. (ii) The quenching of EB bound to ct-DNA by Acr–Cbl nanoparticles is in good agreement with the linear Stern–Volmer equation. (E) (ai–biii) Confocal fluorescence and brightfield images of HeLa cells: (ai–aiii) cells + nonaggregated Acr–Cbl (4×10^{-5} M) after 4 h of incubation: (ai) brightfield image, (aii) fluorescence image and (aiii) overlay image of (ai) and (aii). Cells were incubated with 20 μM Acr–Cbl nanoparticles. (B–E) are reprinted with permission from ref. 37 American Chemical Society.

1.1.3 *p*-Hydroxyphenacyl conjugated benzothiazole: single component photoresponsive fluorescent organic nanoparticles as an environment activatable nanoprodrug with two-step surveillance in anticancer drug release. Recent studies have shown that DDSs which can be localized to cancer and deliver the chemotherapeutic agent on demand resulted in enhanced therapeutic activity. A higher level of intrinsic hydrogen peroxide (5 μM to 1.0 mM) has been observed in cancer cells due to the overproduction of reactive oxygen species (ROS) in comparison to normal cells.[41–46] This exclusive feature of the cancer cell microenvironment provided an advantage toward the development of cancer cell selective chemotherapeutic nano DDSs. Keeping this in mind, our group has developed a microenvironment sensitive nanoprodrug, ANPD-X (Activatable Nano Pro-Drug-X), using a phototrigger *p*-hydroxyphenacyl (*p*HP) group tagged with a benzothiazole moiety for targeted cancer therapy (Fig. 5A).[38] The unique ability of nanoprodrug ANPD-X is its dual surveillance in two successive steps in anticancer drug delivery. In the first step, the nanoprodrug identifies the tumor sites by a fluorescence colour change (signal 1, blue to green fluorescence) using H_2O_2-mediated oxidation of the boronate fluorophore. In the next step, precise spatio-temporal irradiation with light only of identified tumor sites results in the release of anticancer drug chlorambucil. Real time information on drug release was achieved by a second fluorescence colour change (signal 2, green to blue fluorescence). The detection of H_2O_2 and specific activation of ANPD-X (mediated by the boronate trigger) were monitored by the spectral change under physiological conditions by UV-vis and fluorescence spectroscopy (Fig. 5Ba). Interestingly, in the presence of H_2O_2, a dramatic increase of the emission band at 518 nm corresponding to the keto emission (Fig. 5C and Bb) was observed, along with a concomitant decrease in the fluorescence intensity at 448 nm (enol emission) (Fig. 5C). This large bathochromic shift of 70 nm caused a distinct fluorescence colour change from blue to green. The TEM and DLS data showed that ANPD-X nanoparticles were globular in shape with a size of ~78 nm, but after H_2O_2 treatment the particle size was reduced by ~20 nm. On the other hand, with an increase in the irradiation time (0–15 min) a gradual decrease of the intense green emission band was observed along with the appearance of

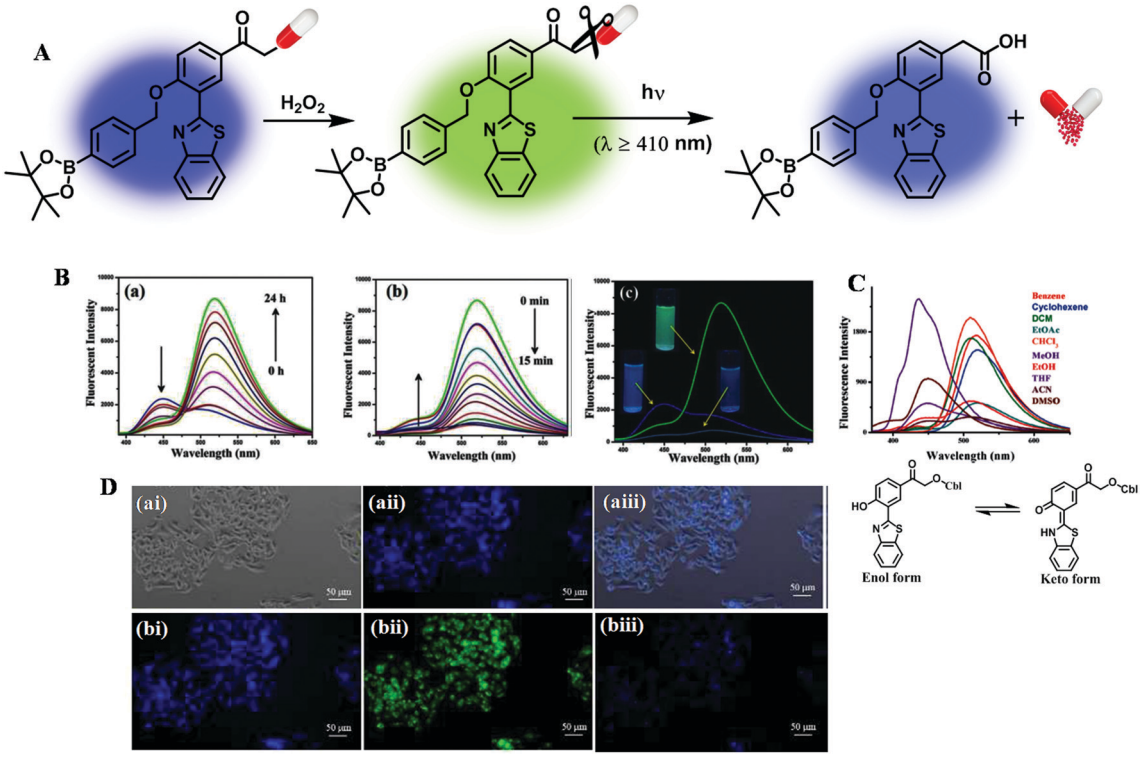

Fig. 5 (A) Schematic representation of the H_2O_2 activable nanoprodrug exhibiting two-step surveillance in drug release. (B) (a) Fluorescence response of ANPD-X against time after addition of H_2O_2 (50 equiv.), (b) change in the fluorescence spectral profile with increasing irradiation time, and (c) comparison of the fluorescence spectral profile in the absence of H_2O_2, in the presence of H_2O_2 and after photoirradiation. (C) Emission spectra of benzothiazole conjugated *p*-hydroxyphenacyl–chlorambucil in different solvents, showing ESIPT. (D) Cellular fluorescence images of HeLa cells after cellular uptake study with ANPD-X: (ai) bright field image, (aii) fluorescence image, and (aiii) merge of the bright field and fluorescence images, and (bi) cells treated with ANPD-X, (bii) ANPD-X pretreated cells after treatment with H_2O_2, and incubating for 12 h, and (biii) after visible light (≥410 nm) irradiation. (B and D) are reprinted with permission from ref. 40. Copyright 2017: American Chemical Society. (C) is reprinted with permission from ref. 40. Copyright 2016: Willey-VCH.

a new blue emission band at 450 nm corresponding to the photoproduct *p*HP-Benz-COOH (Fig. 5Bb and c). The hypsochromic shift in the emission spectra was due to the disruption of conjugation (phenolic hydroxyl group to the carbonyl group) occurring during photolysis. Fascinatingly, ANPD-X showed almost 90% drug release after 15 minutes of visible light irradiation.

The H_2O_2-mediated activation and light triggered release of chlorambucil of nano DDS ANPD-X (Fig. 5D) was performed *in vitro* using HeLa cell lines. MTT assay revealed that enhanced cytotoxicity was noted upon photoirradiation of ANPD-X incubated cells in comparison with *p*HP-Benz–Cbl and chlorambucil because of the efficient bio-distribution of ANPD-X nanoparticles and photorelease of the anticancer drug inside the cancer cells.

Therefore, our single-component organic nanoparticles ANPD-X showed very fascinating properties like good tumor microenvironment sensitivity, high cellular uptake capability and spatiotemporal control over the drug delivery, which made them a highly efficient photoresponsive nano DDS.

1.1.4 *p*-Hydroxyphenacyl conjugated salicylaldazine: single component photoresponsive fluorescent organic nanoparticles showing 'AIE + ESIPT' assisted photorelease for dual anticancer drug delivery with real-time monitoring ability. In recent years, the AIE process has captured great attention since it provides a high signal to noise ratio, excellent photostability in the solution phase and a chance to look into the interesting emission properties of a molecule in the aggregated state.[47,48] AIE fluorogens are highly emissive in their aggregated state but exhibit weak fluorescence in solution. The restricted intramolecular motion in the aggregated state of AIE fluorogens plays a significant role in their photophysical behaviour.[49] To the best of our knowledge, photoresponsive organic nanoparticles as a DDS based on the AIE process have not been developed. Hence, our group designed a photoresponsive nano DDS, which exhibits both AIE and ESIPT phenomena, by simple incorporation of a salicylaldazine moiety into a *p*HP (*p*-hydroxyphenacyl) phototrigger (Fig. 6A).[39] Our newly designed nano DDS (nanoparticulate drug delivery system-5, NDD5) showed excellent properties like (i) the excitation wavelength is extended greater than 410 nm, (ii) it releases drugs only in the aggregated state, (iii) it produces a distinct change in the fluorescence colour on drug release, thus providing immense scope to monitor the drug release profile in real-time (Fig. 6B) and (iv) it has the ability to release two different drugs sequentially so that it can be used effectively in the area of combination chemotherapy (Fig. 6C). Transmission electron microscopy (TEM) revealed that our nano DDS (NDD5) was globular in shape with a size of ∼68 nm (Fig. 6D). It was also

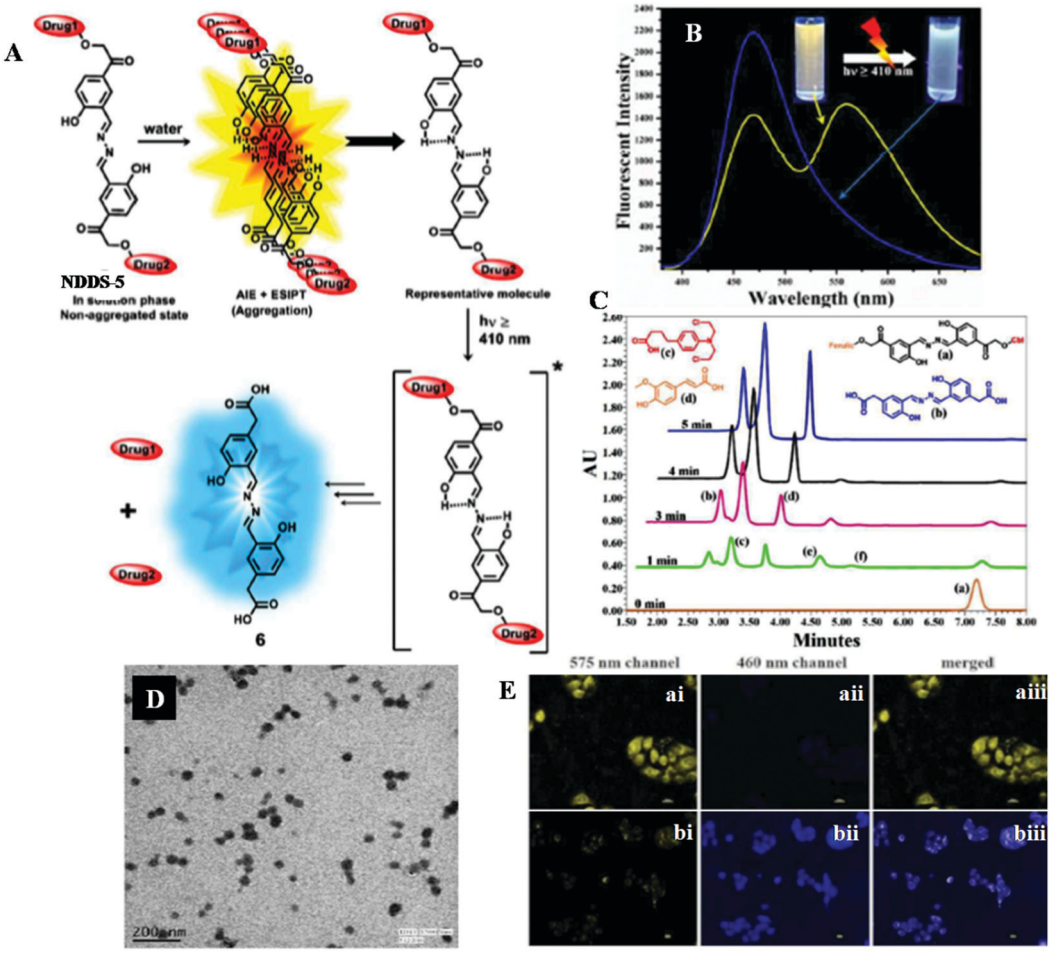

Fig. 6 (A) AIE + ESIPT′ assisted photorelease from NDDS-5. (B) Comparison between the fluorescence spectra of NDDS-5 before and after photolysis (inset: fluorescence colour change during photolysis). (C) HPLC overlay chromatogram of NDDS-5 during photolysis using visible light (≥410 nm) in an ACN–water mixture (f_w = 99 vol%). a = 5, b = photoproduct 6, c = released chlorambucil, d = released ferulic acid, and e and f are singly protected species. (D) TEM images of NDDS-5 before photolysis. (E) Exploration of the real-time (fluorescence confocal images captured at different intervals of time during irradiation) monitoring capability of NDDS-5 during photorelease of drugs upon visible light (≥410 nm) irradiation. Irradiation time: (a) 0 min and (b) 5 min. (A–E) are reprinted from ref. 39: The Royal Society of Chemistry.

noted that our nano DDS NDDS-5 was quite stable in the dark in culture medium but ~90% of one of the caged drugs (chlorambucil and ferulic acid) was released within 5 min of visible light irradiation.

We carried out *in vitro* studies of NDDS-5 using HeLa cells, which showed a uniform distribution of NDDS-5 inside the cells, indicating good cellular internalization. The co-localization experiment revealed that NDDS-5 went selectively into the lysosomes of the HeLa cells. Real time monitoring of drug release by our NDDS-5 was followed through confocal microscopy. We noted that initially the cells exhibited yellow fluorescence due to the internalization of NDDS-5 having an AIE effect (Fig. 6Eai). After 3 min, both yellow and blue fluorescence were observed on exposure to light, intimating partial release of the drugs. The cells showed a complete fluorescence colour change from yellow to blue after 5 min of irradiation with visible light (410 nm), suggesting a greater quantity of photoreleased drugs (chlorambucil and ferulic acid) (Fig. 6Ebii). MTT assay clearly revealed that amplified cytotoxicity was observed upon irradiation of NDDS-5 with respect to free chlorambucil, which was owing to efficient bio-distribution and the synergistic effect of ferulic acid and chlorambucil inside the cancer cells. In short, our nano NDD5 exhibited unique properties like excellent cellular uptake capability, appreciable biocompatibility, and great spatiotemporal precision of the drug release, which makes it an excellent photoresponsive nano DDS for dual release.

1.2 Single component photoresponsive fluorescent organic nanoparticles for microenvironment targeted PDT and combination therapy

Photodynamic therapy (PDT) has emerged as a promising treatment modality for cancer. PDT is a well-established therapeutic causing cellular and tissue damage with spatiotemporal selectivity and specificity.[50,51] In PDT, singlet oxygen acts as a potential killing agent and is generated from the ground state triplet molecular oxygen in the presence of a suitable photosensitizer upon irradiation. Therefore, for

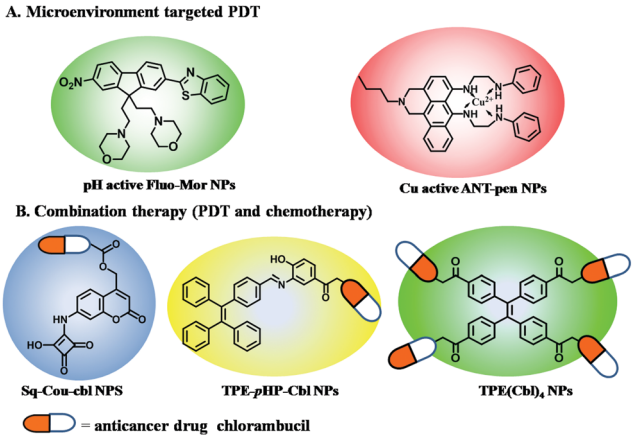

Fig. 7 Single component photoresponsive fluorescent organic NPs for (a) microenvironment targeted PDT and (b) combination therapy (PDT and chemotherapy).

effective singlet oxygen production, apart from light and oxygen, suitable photosensitizers are required. To serve the purpose, inorganic nanoparticles such as Au nanoparticles, graphene oxide, and transition metal oxides have been extensively explored as nanocarriers for PDT agents.[52–54] However, these inorganic nanoparticles are often associated with cytotoxicity, which limits their use in biomedical applications. Hence, our group designed single component fluorescent organic nanoparticle (FONP) based photosensitizers, which can efficiently penetrate and accumulate in cancer cells *via* the EPR effect. With precise modifications in the photosensitizer systems, we achieved effective anticancer activity employing target specific PDT activity and combination therapy (PDT + chemotherapy).

Nowadays, researchers have utilized the difference in the microenvironment between healthy and cancer cells to target and selectively kill cancer cells.[55,56] Considering this fact, we reported a few single component FONPs (Fluo-Mor NPs and ANT-pen NPs, Fig. 7A) to target the microenvironment of cancer cells [*e.g.*, low pH and high Cu(II) concentration] and result in enhanced PDT activity. In this case, the structural modifications of the photosensitizers enable the development of targeted specific PDT efficacy by suitably organizing the excited energy states. We also introduced another strategy of light induced drug release along with PDT by single component fluorescent organic NPs for combination therapy (Fig. 7B). In this section, we will illustrate our efforts to discuss the development of such FONPs and their effectiveness in cancer therapy.

1.2.1 Fluorescent organic nanoparticles for microenvironment targeted PDT

1.2.1.1 Fluorene–morpholine: single-component photoresponsive fluorescent organic nanoparticles for lysosome targeted pH-triggered photodynamic therapy with fluorescence switch on–off. The significantly increased acidity in the lysosome of cancer cells (pH 4.5–5.0) provides a promising pH-sensitive site for pH activatable therapy.[57,58] Keeping this in mind, in 2016 our group designed fluorene-morpholine NPs (Flu-Mor-NPs) (Fig. 8A), for targeted and real-time monitored cancer treatment.[59] In this system, a functionalized fluorene moiety was chosen to construct the nanosystem for the following reasons: (i) strong 2PE absorption to induce NIR-activated PDT, (ii) extended π-conjugation with a push–pull effect, and (iii) moderate hydrophobicity. Functionalization of fluorene with the morpholine unit made it specific to the acidic organelles, *e.g.*, lysosomes (pH 4.0–6.0), of the cells with

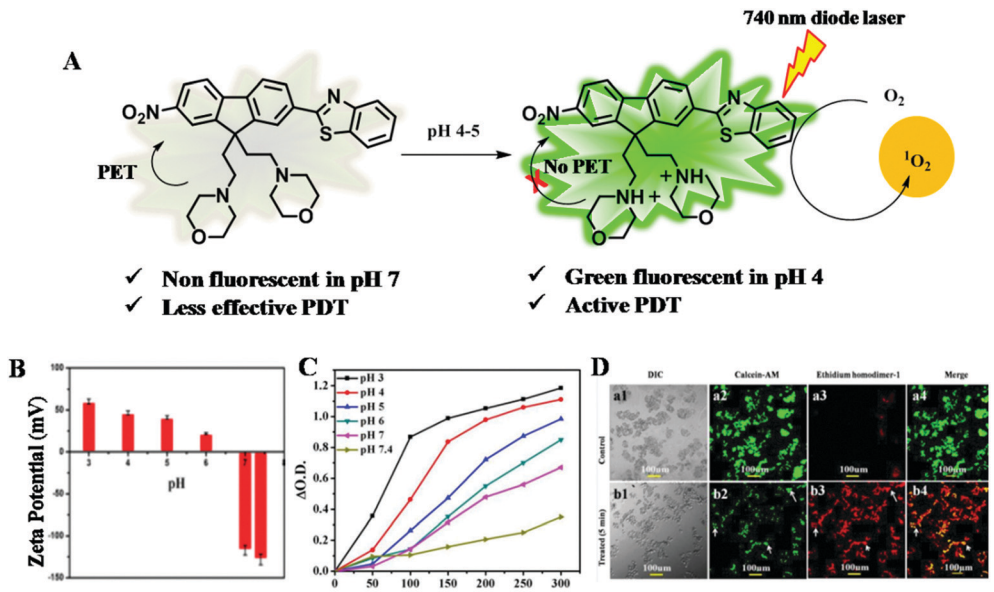

Fig. 8 (A) Fluo-Mor NPs for lysosome targeted PDT. (B) pH-dependent Zeta Potential change in Fluo-Mor organic NPs. (C) Photodegradation study of DPBF (418 nm) in presence of Fluo-Mor NPs at different pH. (D) Live/dead assay for the HT-29 colon cancer cell line in the presence of Fluo-Mor NPs: (a) before irradiation with light, and (b) after 5 min of light irradiation: (1) bright-field images, (2) fluorescence image of calcein AM at 520 nm, (3) fluorescence image of ethidium homodimer 1 at 617 nm, and (4) overlays of the bright-field images and the fluorescence images. Scale bar =100 μm. (B–D) are reprinted from ref. 59: The Royal Society of Chemistry.

pH-regulated fluorescence emission for real-time monitoring of the PDT action.

These NPs were synthesized by a simple reprecipitation technique with a uniform spherical shape of ~43 nm in size. The zeta potential values of the Fluo-Mor NPs were largely positive upon lowering the pH, which in turn helped these NPs to act as an endosomolytic and lysosomolytic pH-responsive PDT agent (Fig. 8B). Interestingly, at neutral pH, morpholine was observed to behave like a donor unit indulging in effective photoinduced electron transfer (PET) to the acceptor fluorene unit, but, in acidic pH, the PET process was quenched, resulting in the turn-on green fluorescence of the fluorene moiety. Accordingly, effective PDT was observed in acidic pH compared to physiological pH.

The $^1O_2$ quantum yields of the Fluo-Mor NPs decreased with increasing pH of the solution. The maximum quantum yield was found in the region of pH 3.0–4.0 (Φ_Δ = 0.65 and 0.58, respectively), whereas the value decreased up to 0.09 at pH 7.4 (Fig. 8C). Thus, the generation of $^1O_2$ by the Fluo-Mor NPs was almost negligible in non-cancerous cells. The live/dead assay with calcein AM and ethidium homodimer-1 showed the loss of cancer cell membrane integrity or membrane rupture, confirming the light triggered cancer cell death (Fig. 8D). Hence, selectively switching the activity of Fluo-Mor NPs under an acidic environment turned on the fluorescence response and also enhanced the cancer cell killing efficiency with minimum side-effects.

1.2.1.2 Anthracene-N-phenylethylenediamine: single component photoresponsive fluorescent organic nanoparticles for a chemosensor of Cu(II) with selective switching on and off photodynamic therapy. Targeting the enhanced copper concentration in cancer cells has emerged as an imperative technique for tumour microenvironment targeted treatment of multiple melanomas.[60] It was known from the literature that the average copper content is 2–3 times higher in cancer-affected patients compared to their healthy counterparts.[61] Hence, a photosensitizer which is otherwise inactive for PDT but could show efficient singlet oxygen generation upon specific coordination with Cu(II) will be an excellent choice for intracellular heterogeneity responsive targeted PDT.

Keeping this in mind, in 2016, we designed fluorescent organic NPs based on anthracene-*N*-phenylethylenediamine (ANT-pen), which selectively detected Cu(II) ions and concurrently exhibited efficient PDT activity only from their Cu(II)-chelation state (Fig. 9A).[62] ANT-pen NPs were also synthesized by a simple reprecipitation technique, being globular in shape and ~37 nm in size. It is noteworthy that the large red shift

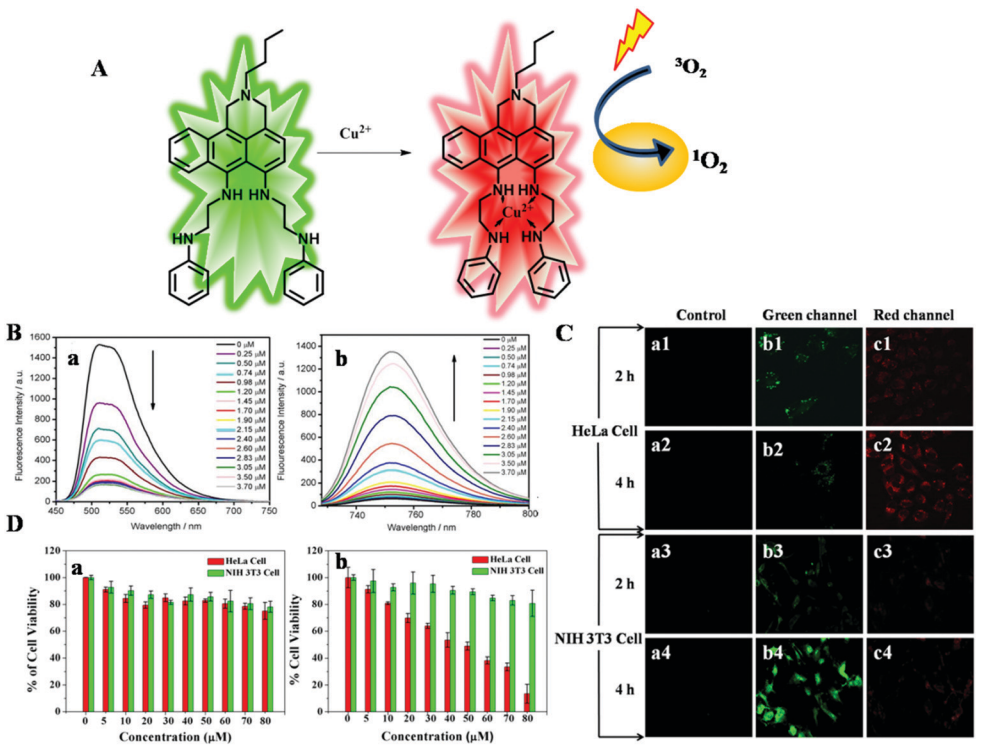

Fig. 9 (A) ANT-pen organic nanosystem for Cu(II) targeted PDT. (B) Fluorescence spectra of ANT-pen NPs (10 mM) with different amounts of Cu(II) (0–2.0 equiv. *i.e.* 0–3.7 mM) in an EtOH-HEPES buffer (60 : 40) solution upon excitation at (a) 450 nm, and (b) 710 nm. (C) Cellular internalization study of ANT-pen NPs (9 mM) in HeLa (a1–c2) and NIH 3T3 cell lines (a3–c4) using confocal microscopy; fluorescence images of ANT-pen NPs in the (a) control, (b) green channel (460 nm emission channel) and (c) red channel (620 nm emission channel) after 2 h (lanes 1 and 3) and 4 h (lanes 2 and 4) incubation. (D) Comparative cell viability study of ANT-pen NPs on HeLa (red bar) and NIH 3T3 cell lines (green bar) (a) before irradiation, and (b) after irradiation for 10 min with visible light (>410 nm) at different concentrations. Values are presented as means ± standard deviations of three different observations. (B–D) are reprinted with permission from ref. 62. Copyright 2016: Wiley-VCH.

(green to red) in fluorescence for the ANT-pen NPs upon complexation with Cu(II) made them useful for real-time monitoring of singlet oxygen generation (Fig. 9B). The comparative studies by confocal laser scanning microscopy (CLSM) analysis between a cancerous HeLa cell line having high Cu(II) concentration and a non-cancerous NIH3T3 cell line having low Cu(II) concentration confirmed the selective sensing property of ANT-pen NPs towards Cu(II) (Fig. 9C).

Also, the comparative *in vitro* biological studies in cancerous HeLa cells and non-cancerous NIH3T3 cells manifested selective cytotoxicity towards HeLa cells (Fig. 9D), owing to the formation of ANT-pen-Cu(II) complexes. Our designed ANT-pen NPs were enabled to visualize the presence of excess Cu(II) in cancer cells and exhibited profound singlet oxygen generation with a quantum yield of 0.70 only upon chelation with Cu^{2+}. Therefore, the ANT-pen NPs showed tumor selectivity by a distinct fluorescence colour change (green to red) method and acted as a potential PDT agent in the presence of Cu(II) in cancer cells. In the above mentioned two studies, we discussed our developed single component FONPs for targeted PDT activity based on the tumour microenvironment *i.e.* lower pH concentration and excess Cu(II) availability in cancer cells. In the next section, we will discuss single component FONPs for combination therapy (PDT and chemotherapy).

1.2.2 Single component photoresponsive fluorescent organic nanoparticles for combination therapy (PDT and chemotherapy). In the last few years, the combination of PDT and chemotherapy using a single nanoplatform has been effectively applied to achieve enhanced therapeutic efficacy with minimal side effects in cancer treatment.[63,64] In particular, combining PDT with chemotherapy is a self-regulating approach since noninvasive PDT and chemotherapy follow two different mechanistic pathways in the destruction of cancer cells.

1.2.2.1 Squaric acid–coumarin–chlorambucil: single component photoresponsive fluorescent organic nanoparticles for self-monitored combination therapy. In 2018, we introduced squaric acid–coumarin–chlorambucil (Sq–cou–cbl) conjugates as single component photoresponsive NPs (Fig. 10A) for combination therapy.[65] Here, a coumarin based phototrigger was chosen for caging the anticancer drug chlorambucil (Cbl), whereas the squarin unit was chosen as a sensitizer for PDT activity. The Sq–Cou–Cbl NPs (photosensitizer–phototrigger nanoconjugate) and Sq–Cou–OH NPs (photoproduct after drug release) were found to be globular in shape with ~60 nm and ~140 nm sizes, respectively.

It is noteworthy that the Sq–Cou–Cbl NPs released chlorambucil in a spatio-temporal manner and generated singlet oxygen upon visible light irradiation. HPLC study showed that nearly 85% anticancer drug was released upon 60 min of irradiation ($\lambda \geq 410$ nm) (Fig. 10B). During photolysis, the blue fluorescence intensity of the Sq–Cou–Cbl NP solution increased by 5 fold owing to the conversion to Sq–Cou–OH NPs. The quantum yield for singlet oxygen generation by Sq–Cou–Cbl NPs and Sq–Cou–OH NPs was monitored by DPBF degradation study and found to be

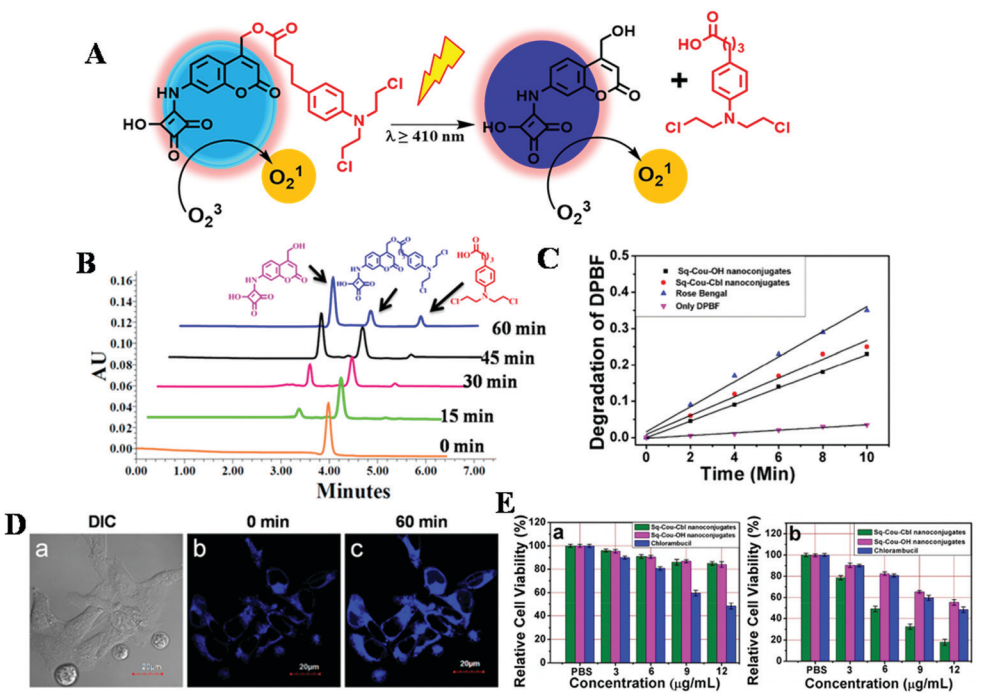

Fig. 10 (A) Combination therapy (anticancer drug + PDT) of Sq–Cou–Cbl upon irradiation. (B) HPLC study for light triggered drug release by Sq–Cou–Cbl nanoparticles. (C) Singlet oxygen generation of Sq–Cou–Cbl and Sq–Cou–OH nanoparticles by DPBF degradation study. (D) Confocal images of internalization of Sq–Cou–Cbl nanoparticles in HeLa cells: (a) DIC (differential interference contrast), (b) before photolysis (0 min), and (c) after photolysis (60 min). Scale bar = 20 μm. (E) Cell viability assay of Sq–Cou–Cbl and Sq–Cou–OH nanoparticles and chlorambucil in the HeLa cell line: (a) before photolysis, and (b) after photolysis. Values are presented as mean ± SD. (B–E) are reprinted with permission from ref. 65. Copyright 2018: American Chemical Society.

0.51 and 0.46, respectively (Fig. 10C). The above study indicates that the photoproduct after the drug release, *i.e.* Sq–Cou–OH NPs, was also able to generate singlet oxygen. Further, abilities like the *in vitro* cellular uptake efficiency (through a lysosomal pathway), singlet oxygen generation, and self-reporting of drug delivery of the Sq–Cou–Cbl NPs were demonstrated by confocal cellular imaging studies (Fig. 10D). The cytotoxicity test revealed that the increased anticancer activity of Sq–Cou–Cbl NPs compared to Sq–Cou–OH NPs was due to the synergistic effect of the released anticancer drug chlorambucil and PDT (Fig. 10E). Interestingly, PDT from the photoproduct Sq–Cou–OH NPs was an additional benefit for improved therapeutic efficacy. Overall, the single-component visible light responsive Sq–Cou–Cbl NPs were found to be highly effective for reducing the cancer cell viability due to the synergistic chemo-photodynamic therapeutic effect.

1.2.2.2 Tetraphenylethylene-p-hydroxyphenacyl–chlorambucil: single component fluorescent organic nanoparticles for chemo-photodynamic therapy with real time cellular imaging. We have discussed the advantages of incorporating AIE + ESIPT phenomena in the construction of drug delivery systems. In continuation, in the year 2018, we developed an AIE based nanosystem (TPE–*p*HP–Cbl NPs) by combining tetraphenylethylene and a *p*-hydroxyphenacyl phototrigger for the combination of PDT and chemotherapy (Fig. 11A).[66]

The TPE–*p*HP–Cbl NPs were synthesized by the reprecipitation technique from the TPE–*p*HP–Cbl conjugate. HR-TEM revealed that the nanoparticles were spherical and ~38 nm in size. The yellow fluorescence of TPE–*p*HP–Cbl NPs was found to be increased with an increase in the water fraction as a result of the AIE phenomenon (Fig. 11Ba). Most importantly, the TPE–*p*HP–Cbl NPs showed a fluorescence colour change (yellow to green) on photolysis, thus helping in real-time visualization of drug release by fluorescence imaging. The blue shift of the emission spectra was due to the disruption of the conjugation from the –OH moiety to the keto group of TPE–*p*HP–Cbl NPs.

The HPLC study confirmed that ~90% drug was released by TPE–*p*HP–Cbl NPs within 5 min of irradiation under visible light ($\lambda \geq 410$ nm) (Fig. 11C). The singlet oxygen generation quantum yield was found to be 0.28 and 0.24 for TPE–*p*HP–Cbl NPs and TPE–*p*HP–OH NPs (photoproduct), respectively (Fig. 11D). The *in vitro* cell imaging study confirmed the real-time monitoring drug release ability of TPE–*p*HP–Cbl NPs. As expected, before irradiation, the confocal image exhibited a yellow fluorescence colour of TPE–*p*HP–Cbl NPs due to the AIE effect, while after irradiation a green fluorescence colour was observed due to the disruption in conjugation (Fig. 11E). The significant features of the TPE–*p*HP–Cbl NPs are the real-time monitoring ability during drug release, and enhanced PDT activity due to singlet oxygen generation by the photoproduct.

1.2.2.3 Four armed tetraphenylethylene: single component fluorescent organic nanoparticles for chemo-photodynamic therapy and cellular imaging. In the same way, in 2019, we developed visible light-responsive FONPs, tetraphenylethelene–chlorambucil [TPE(Cbl)$_4$], using the TPE chromophore for an improved combination of chemo-photodynamic therapy (Fig. 12A).[67] The most interesting feature of this work was the release of 4 equivalents of active drugs from a single nanosystem along with PDT activity, which potentially increased the therapeutic

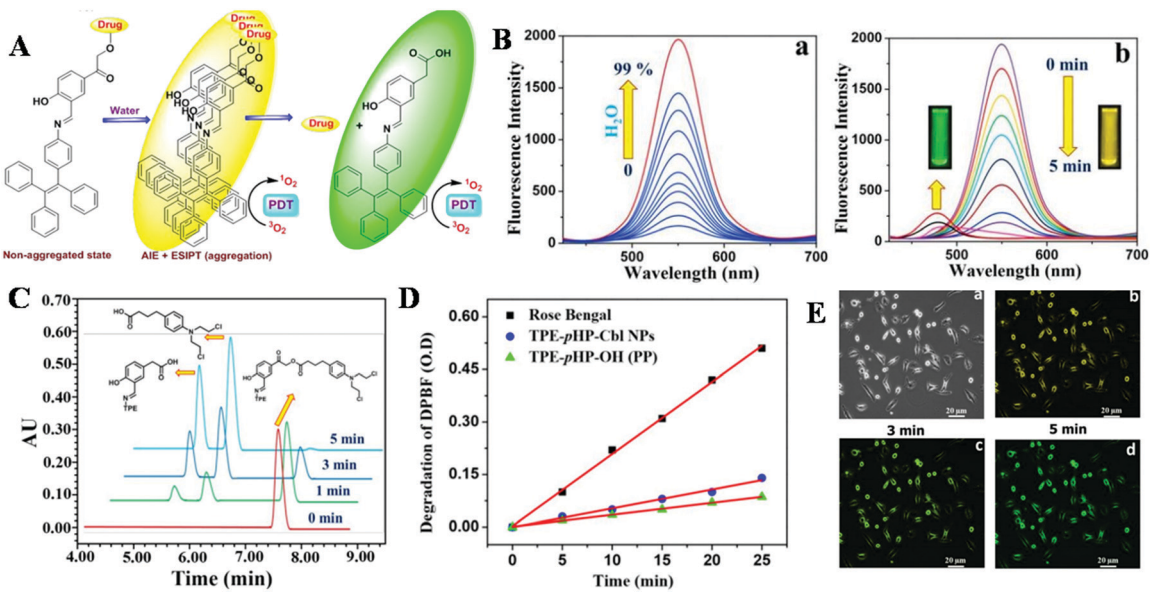

Fig. 11 (A) AIE–ESIPT based fluorescent TPE–*p*HP–Cbl NPs for combination therapy. (B) (a) The yellow fluorescence intensity of TPE–*p*HP–Cbl NPs increases with an increase in the water fraction and (b) the fluorescence color change (yellow to green) of TPE–*p*HP–Cbl NPs upon photoirradiation. (C) Photorelease of the drug (chlorambucil) by TPE–*p*HP–Cbl NPs upon irradiation. (D) Singlet oxygen generation of TPE–*p*HP–Cbl NPs and TPE–*p*HP–OH NPs by DPBF degradation study. (E) Confocal microscopy images captured at different intervals of time during irradiation of TPE–*p*HP–Cbl NPs in HeLa cells: (a) bright-field image, (b) 0 min, (c) 3 min and (d) 5 min. Scale bar = 20 μm. (A–E) are reprinted with permission from ref. 66. Copyright 2018: American Chemical Society.

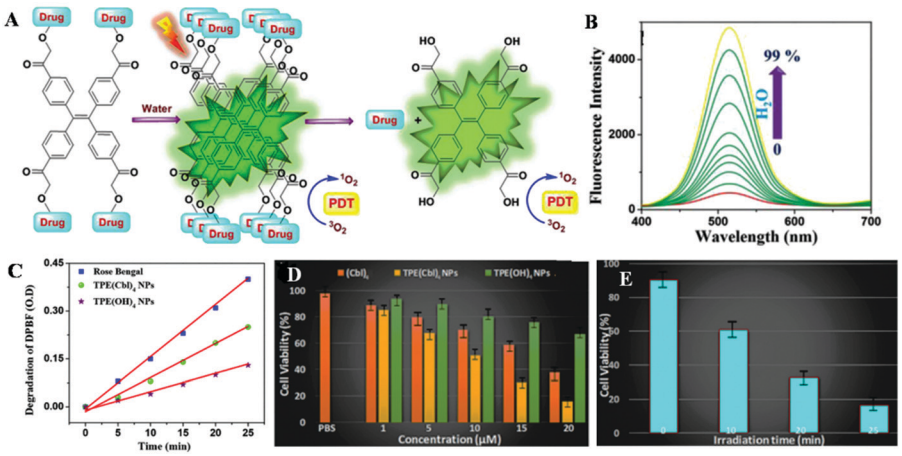

Fig. 12 (A) "AIE"-based TPE(Cbl)$_4$ nanoparticles for combination (chemo-photodynamic) therapy. (B) Increase in the green fluorescence intensity of TPE(Cbl)$_4$ with an increase in the water fraction. (C) Singlet oxygen generation of TPE(Cbl)$_4$ NPs and TPE(OH)$_4$ NPs by DPBF degradation study. (D) Cell viability assay of (Cbl)$_4$, TPE(Cbl)$_4$ NPs, and TPE(OH)$_4$ NPs in the cancer cell line after photoirradiation. (E) Cell viability assay study of TPE(Cbl)$_4$ NPs at different time intervals of photoirradiation. (A–E) are reprinted with permission from ref. 67. Copyright 2019: American Chemical Society.

efficacy by lowering the drug dose. The TPE(Cbl)$_4$ NPs were spherical in shape with a ~42 nm size, synthesized by the same reprecipitation technique from the TPE(Cbl)$_4$ conjugate. The TPE(Cbl)$_4$ NPs displayed strong green fluorescence with an increase in the water fraction because of the AIE effect (Fig. 12B). Upon exposure to visible light ($\lambda \geq 410$ nm), our TPE(Cbl)$_4$ NPs simultaneously produced singlet oxygen and uncaged 4 equivalents of the anticancer drug sequentially in their aggregated state (Fig. 12C). On the other hand, the formed photoproduct also exhibited PDT activity upon light irradiation, which was an added advantage for effective anticancer activity. *In vitro* studies exhibited properties like self-tracking, cellular imaging, photoregulated synergistic chemo-photodynamic therapy, and biocompatibility of TPE(Cbl)$_4$ NPs (Fig. 12D and E).

Overall, the above discussed fluorescent organic TPE(Cbl)$_4$ NPs exhibited unique properties like appreciable biocompatibility and simultaneous singlet oxygen generation with four equivalents of anticancer drug release, making them a potential combination therapeutic agent for cancer treatment.

2 Single component photoresponsive fluorescent organic nanoparticles as a gasotransmitter donor

Of late, biological functions of gasotransmitters have captured great attention in the scientific community. Although they are not recognized as classical signaling molecules, still they regulate a number of important cellular functions through complex chemical interactions with each other (including metabolites) and targeting proteins. Gasotransmitters control various physiological functions, including regulation of the cardiovascular, nervous, gastrointestinal, excretory, and immune systems, and many other cellular functions, including apoptosis, proliferation, inflammation, cell metabolism, gene transcription, *etc.*[68] Nitric oxide (NO), carbon monoxide (CO), and hydrogen sulfide (H_2S) are a family of molecules known as gasotransmitters.[69] Cell signalling by gasotransmitters is mostly complex and is dependent on their local concentration. This indicates the need for controlled generation of gasotransmitters under physiological conditions. However, site specific controlled administration of gasotransmitters to their target sites in the physiological environment is challenging because of their high diffusion rate and low solubility in blood. This problem was eliminated using light-responsive gasotransmitter donors.[70,71]

Hence, our group developed single component fluorescent organic nanoparticles for regulated release of gasotransmitters (H_2S and NO) with enhanced transportation and "on-demand" "tunable" release (Fig. 13).

2.1 Tetraphenylethylene conjugated *p*-hydroxyphenacyl: single component fluorescent organic nanoparticles for the release of hydrogen sulfide with real-time cellular imaging

H_2S has a wide range of physiological functions such as anti inflammatory, antioxidative, vasodialation and cytoprotective effects.[72,73] H_2S has tunable activity depending on the concentration: at low concentrations it has cytoprotective ability against cellular damage, while at higher concentrations it

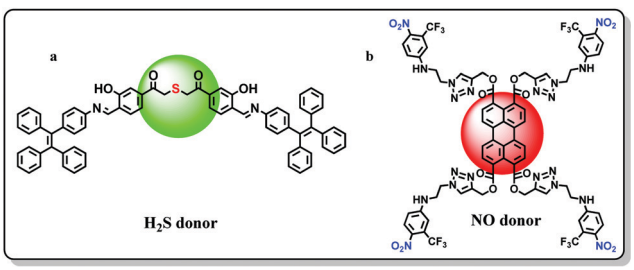

Fig. 13 Single component light responsive fluorescent organic nanoparticles for regulated release of (a) H_2S and (b) NO.

exhibits cytotoxicity. Hence, the monitoring of H_2S release is necessary for treatment.

In 2018, we developed visible light activatable single component FONPs by integrating a tetraphenylethylene (TPE) moiety and *p*-hydroxyphenacyl (*p*HP) phototrigger for the release of hydrogen sulfide (H_2S) with real time monitoring ability (Fig. 14A).[74] Our TPE–*p*HP–H_2S NPs provided advantages like (i) aggregation-induced emission enhancement, (ii) a large Stokes shift, (iii) an excitation wavelength extended to >410 nm, (iv) unlocking of photorelease of H_2S in the aggregated state, (v) real-time monitoring of H_2S release by a simple fluorescence colour change, and (vi) no requirement of an additional reagent for the release of H_2S.

The TPE–*p*HP–H_2S NPs were synthesized by the reprecipitation technique from the TPE–*p*HP–H_2S conjugate. HR-TEM revealed that the nanoparticles were spherical in shape with a ~35 nm size. Irradiation of TPE–*p*HP–H_2S NPs under visible light ($\lambda \geq 410$ nm) released H_2S only in the aggregated state *via* ESIPT assisted photo-Favorskii rearrangement. Methylene blue assay showed that 100 μM of TPE–*p*HP–H_2S NPs released ~40 μM of H_2S after 20 min of irradiation. Our TPE–*p*HP–H_2S NPs aided in real-time monitoring of photorelease of H_2S by a fluorescence colour change (yellow to blue) (Fig. 14B).

The cellular uptake and real-time monitoring of H_2S release from the TPE–*p*HP–H_2S NPs was established *in vitro* using cervical cancer cells (Fig. 14C). MTT assay clearly suggested that there was no inhibition of proliferation of HeLa cells by the TPE–*p*HP–H_2S NPs before and after photolysis, which clearly shows that the H_2S donor TPE–*p*HP–H_2S NPs are not cytotoxic at the studied concentration. Therefore, the TPE–*p*HP–H_2S NPs demonstrated the controlled and real time release of H_2S under visible light without the help of any external agent.

2.2 Perylenetetracarboxylate ester: single component NIR fluorescent organic nanoparticles for photoinduced nitric oxide delivery with self monitoring and real time reporting abilities

The therapeutic efficacy of nitric oxide (NO) is found to be a dual-edged sword like H_2S: in high concentrations, NO is cytotoxic and is used to treat cancer, while in low concentrations it promotes tumor growth. Therefore, on-demand spatiotemporal NO release has captured great attention.[75] In this regard, several photoresponsive NO-donating nanoparticulate systems based on metallic, up-conversion NPs *etc.* have been developed. Since the activity of NO is concentration-dependent, it is absolutely necessary to estimate the amount of NO release. To solve this problem, photoresponsive NO donor NPs with the ability to release along with fluorescence reporting were developed. In this context, our group developed nitric oxide photodonor (NOD) conjugated perylenetetracarboxylate ester (TPT) based fluorescent organic nanoparticles, TPT$(NOD)_4$, with aggregation induced NIR emission for photoinduced nitric oxide delivery along with a red to green emission transition (Fig. 15A).[76] Fluorescent TPT-$(NOD)_4$ NPs were prepared *via* a reprecipitation technique, and their sizes were determined from TEM and DLS studies. From TEM images it was observed that the TPT-$(NOD)_4$ NPs were globular in shape, with an average diameter of ~55 nm (Fig. 15B), whereas from a DLS study the average size of the TPT-$(NOD)_4$ NPs was found to be ~60 nm. These NPs have a zeta potential of +58 mV, representing the surface charge of the NPs. Further, the polydispersity of the

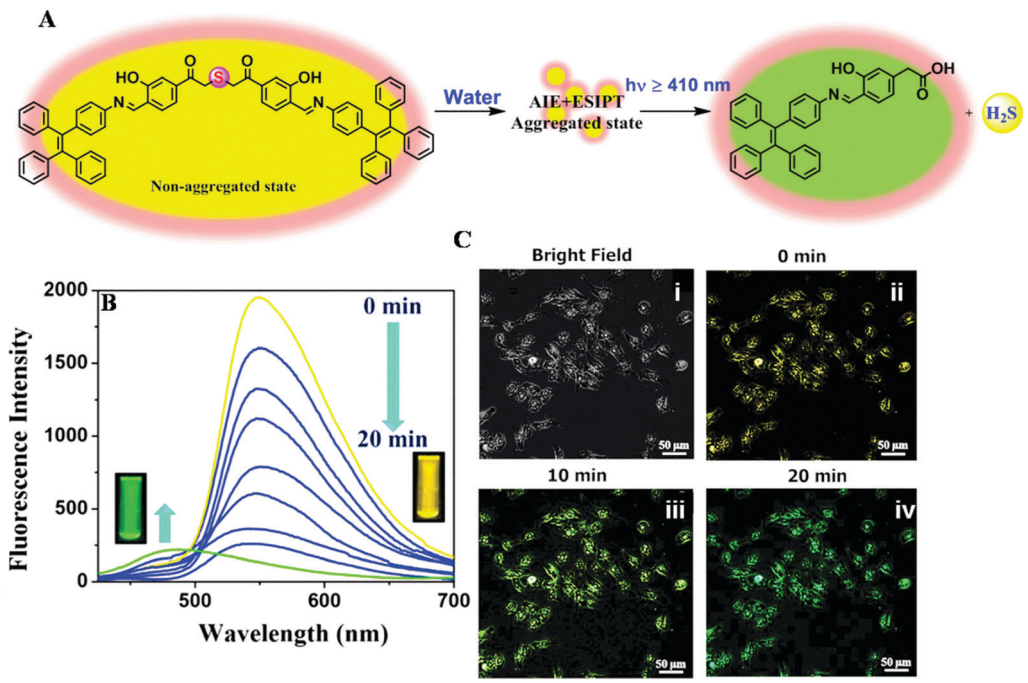

Fig. 14 (A) AIE and ESIPT assisted H_2S release from TPE–*p*HP–H_2S NPs. (B) Fluorescent spectral change of the TPE–*p*HP–H_2S NP donor during photolysis at regular intervals of time (0–20 min). (C) Confocal microscopy images of internalization of the TPE–*p*HP–H_2S NP donor in HeLa cells: (i) bright-field image, (ii) 0 min, (iii) 10 min and (iv) 20 min. Scale bar = 50 μm. (B and C) are reprinted from ref. 74: The Royal Society of Chemistry.

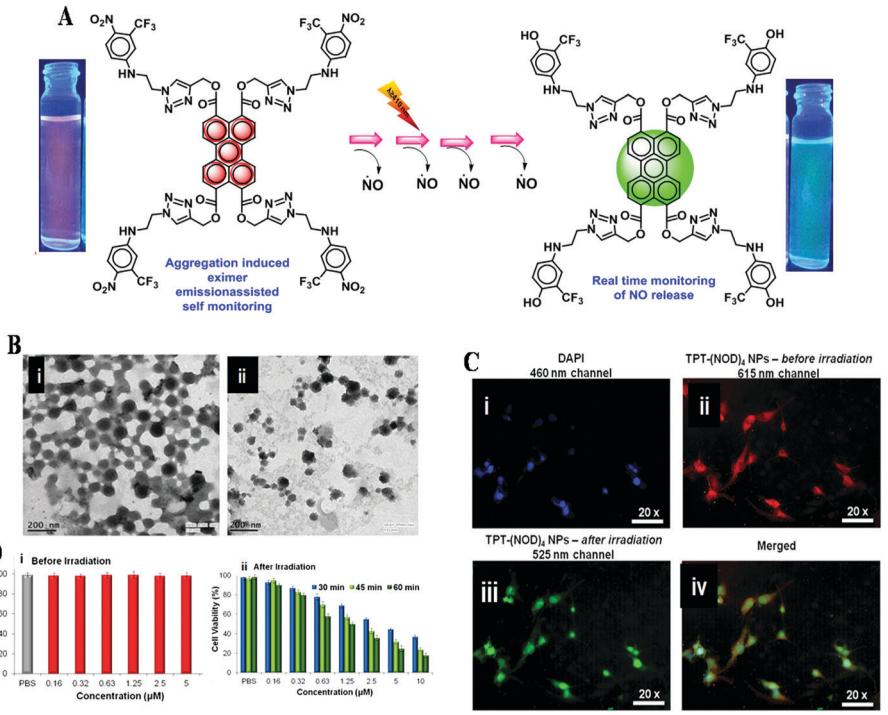

Fig. 15 (A) The working principle of the NO photodonor [TPT $(NOD)_4$ NPs] with self monitoring internalization and real time monitoring of NO release. (B) TEM images of TPT-$(NOD)_4$ NPs, (i) before photolysis, and (ii) after photolysis. (C) Confocal images of U87MG cells, incubated with DAPI for nuclear staining and 6 mM TPT-$(NOD)_4$ NPs, obtained during exposure to visible light irradiation: (i) DAPI nucleus staining; (ii) 0 min – excimer emission (red fluorescence); (iii) 30 min – monomer emission; and (iv) a merged image. (D) Dose-dependent photoinduced anticancer activity of TPT-$(NOD)_4$ NPs, obtained (i) before irradiation and (ii) after irradiation. The values are presented as means ± standard deviations from three different observations. (B–D) are reprinted from ref. 76: The Royal Society of Chemistry.

TPT-$(NOD)_4$ NPs was measured to be 0.144, indicating the uniformity and monomodal dispersion of the NPs in aqueous solution. Importantly, the emission spectrum of TPT-$(NOD)_4$ showed monomer emission, whereas the TPT-$(NOD)_4$ nanoparticles exhibited red-shifted 627 nm emission, which was attributed to aggregation induced excimer emission. Interestingly, our spherical TPT-$(NOD)_4$ NPs exhibited red emission, and upon photolysis using visible light they released NO with a concomitant shift in fluorescence from red to green. The excimer (NIR) emission of TPT-$(NOD)_4$ NPs was utilised in monitoring the cellular internalization of these NPs in U87MG cells. Further, the NO photorelease associated dual colour fluorescence transition was exploited for the real time reporting of NO release inside the cells (Fig. 15C). MTT assay showed high cytotoxicity in HeLa cells for our TPT-$(NOD)_4$ NPs, which is due to the controlled release of 4 equivalents of NO (Fig. 15D). Thus, our TPT-$(NOD)_4$ NPs were the first reported organic nanoparticulate system that can self-monitor *in vitro* cellular internalization and report photoinduced nitric oxide delivery in real time.

3 Single component photoresponsive organic nanoparticles as a drug delivery system for antibacterial treatment

Bacterial infection has become a serious threat to public health globally owing to the numerous problems created by it, such as contamination of medical devices, food spoilage, equipment contamination, multi-drug resistance *etc.*[77] The use of excessive antibiotic agents causes the problem of drug resistance and leads to several side effects due to overdoses.[78] In this context, stimuli-responsive antibiotic-loaded nanoparticles with improved therapeutic efficacy were developed.[79] Within the reported system, the light-responsive bicomponent nano DDS seems to be much more effective as it provides a higher degree of spatio-temporal control during the drug release. However, the main concerns about these systems are the (i) biocompatibility, (ii) real-time tracking ability and (iii) drug loading efficiency, which depends on the nanoparticle surface. All these shortcomings can be addressed if we use single component fluorescent organic nanoparticle systems, because of their inherent advantageous properties as discussed previously.

3.1 1-Acetylpyrene–salicylic acid: single component photoresponsive fluorescent organic nanoparticles for the regulated release of a natural antimicrobial compound, salicylic acid

In 2014, we developed 1-acetylpyrene (AcPy) as single component photoresponsive FONPs for the regulated *in vitro* release of a natural antimicrobial agent salicylic acid (SA) under visible light irradiation ($\lambda \geq 410$ nm) (Fig. 16A).[80] AcPy–SA NPs were prepared from the AcPy–SA conjugate by a simple reprecipitation technique. TEM analysis revealed that the photoresponsive AcPy–SA NPs were ~68 nm in size. Photophysical studies

showed that the AcPy–SA NPs exhibited good fluorescence and absorbance above 400 nm. The zeta potential of the AcPy–SA NPs was about −48.8 mV (Fig. 16B). The high negative zeta potential value indicated that the AcPy–SA NPs were sufficiently stable in aqueous dispersions and can be used for *in vitro* antimicrobial drug delivery. AcPy–SA NPs dispersed in aqueous solution released 90% of salicylic acid in 1 h on irradiation with visible light (≥410 nm) (Fig. 16C).

Both the broth dilution method and live/dead Baclight viability stain studies showed that the AcPy–SA NPs kill bacterial cells upon exposure to visible-light irradiation (≥410 nm) (Fig. 16D). Finally, a change in the topography of the bacterial cell membrane by AcPy–SA NPs upon visible-light irradiation was studied using FESEM and AFM. From the FESEM images (Fig. 16E) it was found that nanoparticles adhere to the surface of the bacterial cells (Fig. 16Ef) and lead to cell-lysis of the bacterial cells when exposed to visible light (Fig. 16Ed and e). The high resolution AFM revealed that the binding of AcPy–SA NPs caused a progressive increase in surface roughness (from 66.86 nm to 228.97 nm). AFM analysis also showed that AcPy–SA NPs which were bound to a bacterial cell membrane appeared with a different surface topography (Fig. 16F) after irradiation with visible light. Hence, the development of such photoresponsive fluorescent organic NPs will be highly beneficial for targeted and regulated antimicrobial drug release because of their biocompatible nature, efficient cellular uptake, and light-induced drug release ability.

4 Single component photoresponsive fluorescent organic nanoparticles as a drug delivery system for agrochemical release

Using excess pesticides on plants leads to many undesirable side effects, including phototoxicity and environmental

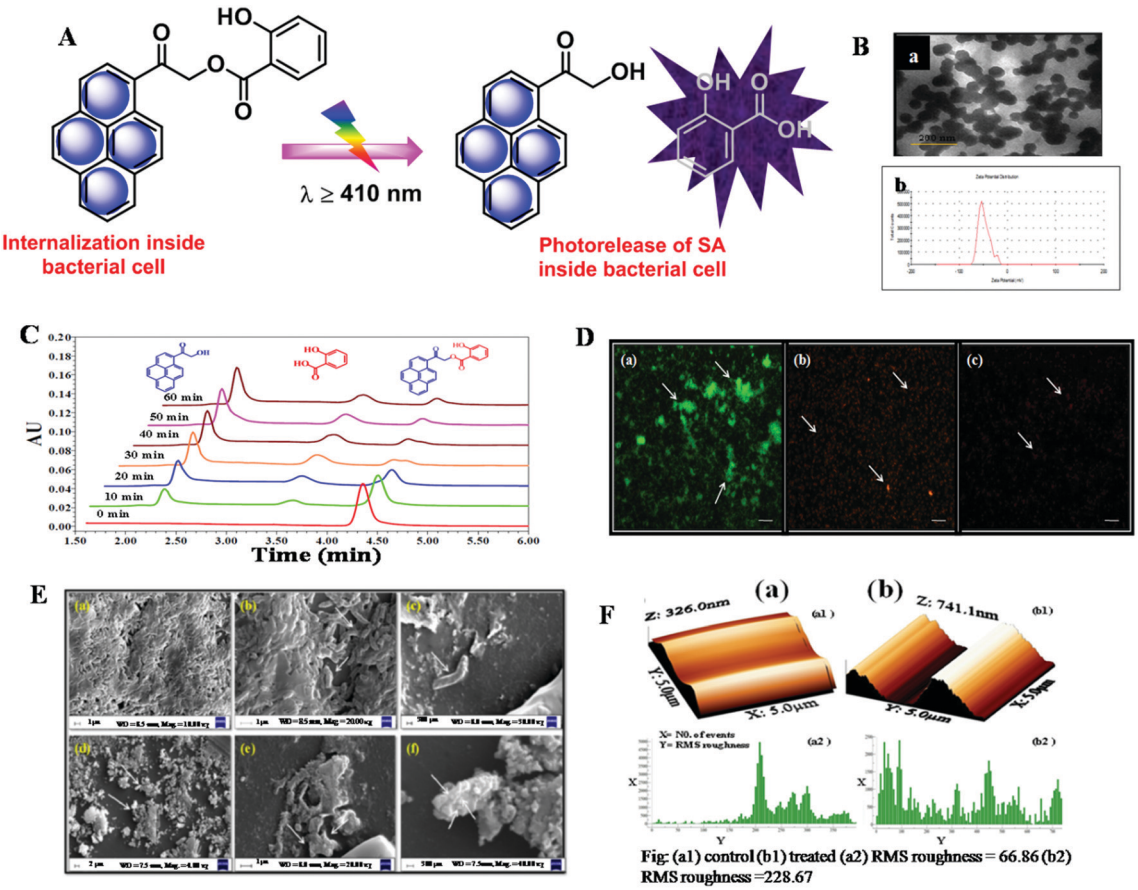

Fig. 16 (A) Working principle of AcPy–SA NPs inside bacterial cells. (B) TEM and DLS studies of AcPy–SA NPs. (C) HPLC overlay chromatogram of AcPy–SA nanoparticles at different intervals of light irradiation (≥410 nm). (D) Live/dead Baclight bacterial viability assay on *Pseudomonas aeruginosa*-ATCC 27853 ((a): control; and (b and c): treated with AcPy–SA nanoparticles (0.5×10^{-6} M) after 10 min and 20 min visible light irradiation, respectively). Imaging was done using a fluorescence microscope (IX 51, Olympus) with a high-performance CCD camera and Image-Pro discovery 5.1 software. Scale bar represent 10 μm. (E) FE-SEM micrograph of *Pseudomonas aeruginosa*-ATCC 27853 ((a–c): control; and (d–f): treated with visible light in the presence of AcPy–SA nanoparticles). (F) Atomic force microscopy view of *Pseudomonas aeruginosa*-ATCC 27853. Images were captured using a scanning probe microscope, Multiview-1000TM, at a scan rate of 0.8–1.0 Hz, and were first-order flattened. The bacteria appear to be hydrated and the outer surface appears (a) smooth for bacteria grown without NPs and (b) a rough surface treated with visible light in the presence of AcPy–SA NPs. (B–F) are reprinted with permission from ref. 80. Copyright 2014: American Chemical Society.

pollution.[81] Here, the concept of controlled release formulations (CRFs) of pesticides has gained a lot of interest as they allow the use of minimum amounts of pesticides for the same period of time, thereby reducing the risk of environmental pollution. Within the various strategies of CRFs, nano-pesticide formulations have recently gained considerable importance in agriculture as they offer unique advantages such as (i) increasing the solubility of poorly soluble pesticides, (ii) slow/targeted release of pesticides and (iii) protecting pesticides against premature release and degradation.[82] The main goal in developing nano-pesticide formulations is to develop intelligent nanocarriers that contain properties such as fluorescence, targeting ability, and precise control of pesticide release. To date, several nanocarriers have been developed for the delivery of pesticides based on polymeric nanoparticles, solid lipid nanoparticles, mesoporous silica nanoparticles, metals, and metal oxide nanoparticles. Although the reported nanopesticide formulations exhibited low toxicity and good biocompatibility, their use is mainly limited as they are incapable of monitoring the amount of pesticides released and tracking the morphological changes occurring in the plants after pesticide release.[83] In this context, we intend to develop light responsive nanopesticide formulations based on fluorescent organic nanoparticles that can provide the following advantages: the ability to (i) visualize and track the transportation and deposition of nanopesticides within the plant system, (ii) help to monitor the morphological changes induced by nanopesticides for the plant, and (iii) have precise control over the release of pesticides, including location, timing, and doses.

4.1 Perylene-3-yl methanol: single component photoresponsive fluorescent organic photoresponsive nanoparticles for controlled release of 2,4-D and real time monitoring of morphological changes induced by 2,4-D in plant systems

For the first time, our group developed a nano-pesticide formulation of 2,4-D using perylene-3-yl methanol as a nanocarrier for performing dual abilities: (i) tracking of morphological changes induced by the pesticide 2,4-D and (ii) controlled release of 2,4-D (Fig. 17A).[84] Pe-2,4-D nano-pesticides and perylen-3-ylmethanol nanoparticles were prepared using a similar reprecipitation technique. TEM images showed that the Pe-2,4-D nano-pesticides and perylen-3-ylmethanol nanoparticles were globular in shape with an average particle size of ~25 nm and ~10 nm, respectively (Fig. 17B). The broad absorption of the Pe-2,4-D nano-pesticides from 350 nm to 550 nm and strong emission at 625 nm indicated that our nano-pesticides can be used for both cell imaging (Fig. 17C) and the regulated release of 2,4-D under visible light irradiation. The distinct fluorescence colour change on photolysis of the Pe-2,4-D nano-pesticides was exploited for real time monitoring of 2,4-D release inside the plant (Fig. 17D). A ten day growth experiment using different concentrations (10^{-4} to 10^{-6} M) of Pe-2,4-D nano-pesticides manifested the growth inhibition effect

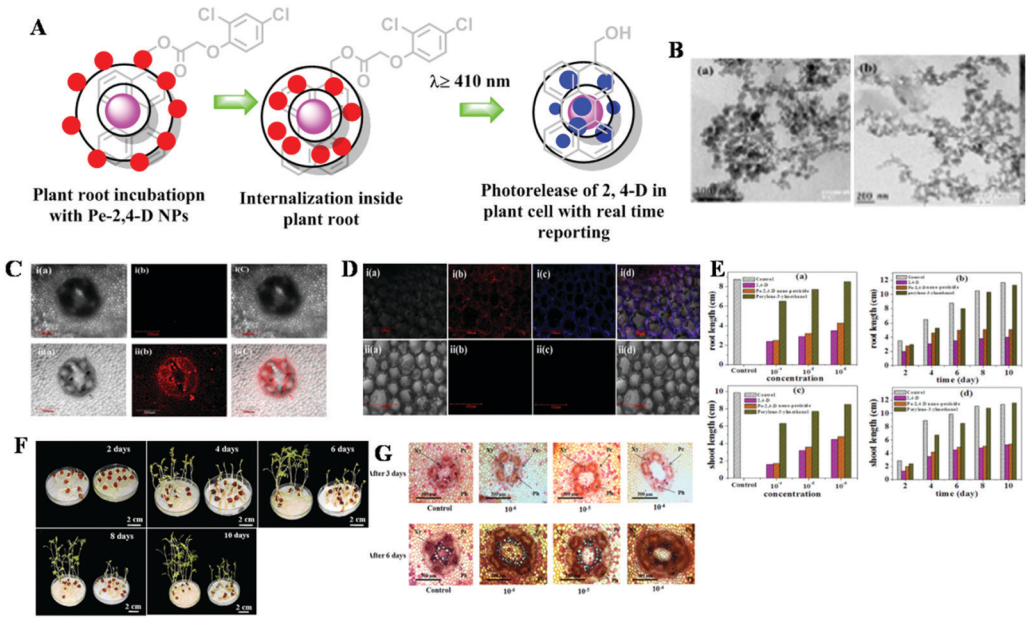

Fig. 17 (A) Working principle of Pe-2,4-D nano-pesticides in plant cells. (B) TEM analysis of Pe-2,4-D nano-pesticides (a) before and (b) after photolysis. (C) Confocal fluorescence and brightfield images of the plant root cross section under (i) control conditions and (ii) treatment with 2×10^{-6} M Pe-2,4-D nano-pesticide in the dark for 6 h [(a) brightfield, (b) fluorescence and (c) overlay]. (D) Confocal microscope images showing real time nano-pesticide release in plants under (i) 15 min irradiation (≥410 nm) after treatment with 2×10^{-6} M Pe-2,4-D nano-pesticide in the dark for 6 h and (ii) control conditions [(a) brightfield, (b) fluorescence (625 nm emission channels), (c) fluorescence (445 nm emission channels) and (d) overlay]. (E) Effect of 2,4-D, Pe-2,4-D nano-pesticides and perylene-3-ylmethanol nano-particles (10^{-4} to 10^{-6} M) on the root and shoot length of *C. Arietinum* at regular time intervals. (F) Effect of 6×10^{-6} M Pe-2,4-D nano-pesticides after regular time intervals of irradiation under visible light (in each set the left side represents the control and the right side the treatment). (G) Anatomical changes induced in the root tissues of *C. Arietinum* by photoreleased 2,4-D (10^{-6} to 10^{-4} M). Here Pc, Ph and Xy represent the pericycle, phloem and xylem, respectively. (B–G) are reprinted from ref. 84: The Royal Society of Chemistry.

Table 1 Photophysical and photochemical properties of phototriggers used as FONPs

Phototrigger	Irradiation wavelength (125 W)	Quantum yield			Real-time monitoring[d]	Ref.
		ϕ_F[a]	Φ_P[b]	ϕ_Δ[c]		
Perylene-3-ylmethyl	≥410 nm	0.9	0.09	—	O	36 and 84
Acridin-9-methyl	≥365 nm	0.03	0.02	—	NO	37
Benzothiazole conjugated *p*-hydroxyphenacyl	≥410 nm	—	0.46	—	O	38
Salicylaldazine conjugated *p*-hydroxyphenacyl	≥410 nm	—	0.48	—	O	39
Fluorene–morpholine	≥365 and 740 nm	—	—	0.65 (≥365 nm)	O	59
Anthracene-*N*-phenylethylenediamine	≥410 nm	—	—	0.70	O	62
Squaric acid–coumarinyl	≥410 nm	0.039	0.083	0.51	NO	65
Tetraphenylethylene-*p*-hydroxyphenacyl	≥410 nm	—	0.51	0.28	O	66
Four armed tetraphenylethylene *p*-hydroxyphenacyl	≥410 nm	—	0.52	0.31	NO	67
1-Acetylpyrene	≥410 nm	0.04	0.39	—	NO	80

[a] Fluorescence quantum yield using quinine sulphate/9,10 diphenyl anthracene as a standard. [b] Photochemical quantum yield for the release of bioactive molecules using potassium ferrioxalate as an actinometer. [c] Singlet oxygen generation quantum yield using rose bengal as a standard (error limit within ±5). [d] Fluorescence color change during photorelease; O = observed, NO = not observed.

of released 2,4-D on the root and shoot systems of brown pea (*C. arietinum*) plants (Fig. 17E). Further, our Pe-2,4-D nano-pesticides helped us to track the anatomical changes in root tissues induced by released 2,4-D. The development of the roots was almost completely inhibited after 6 days of treatment with the nano-pesticides although the roots of the control plants appeared to be healthy and well grown (Fig. 17F). Additionally, we also observed a change in the phloem structure and a cell death like phenomenon in the root tip regions of brown pea seeds (Fig. 17G). Thus, our newly developed nano-pesticide formulation provided the following advantages compared to the simple 2,4-D, like (i) it was easily absorbed by plant cells because of its nano size, (ii) it was formulated in water so that it can overcome the limitation of low water solubility of 2,4-D and (iii) it exhibited a distinct fluorescence colour change of Pe-2,4-D nano-pesticides upon irradiation that was utilized for real time monitoring of 2,4-D release.

Finally, we have summarized in a table the different properties of phototriggers used as FONPs including the wavelength of light used for excitation, fluorescence quantum yield, photochemical quantum yield for deprotection, singlet oxygen generation, and real time monitoring ability (Table 1).

5. Conclusions

In summary, we have shown that light responsive single component fluorescent organic nanoparticles can act as efficient drug delivery systems (DDSs). Light responsive FONPs can be easily prepared from their corresponding conjugates using a simple reprecipitation technique. The light responsive FONPs prepared using the reprecipitation technique were mostly in the range of 20–60 nm. The absorption and emission behaviour of these FONPs was strikingly different from their corresponding conjugates. Light responsive FONPs provide the advantage of releasing the biological molecules in physiological medium, curtailing the limitation of solubility of photocages in aqueous medium. The most remarkable property of these light responsive FONPs is their change in fluorescence colour during photolysis, which was utilised for the real time monitoring of drug release inside cells. *In vitro* studies clearly suggest that using prodrugs in the form of light responsive FONPs provided important advantages like (i) excellent biocompatibility, (ii) efficient cellular internalization, (iii) real time monitoring of drug release inside the cells and (iv) enhanced cytotoxicity due to regulated release of bioactive molecule inside the cells.

Future work

Despite the emerging progress on light responsive FONPs, there are still many challenges in order to fulfil their potential applications. For instance, these nanoparticles should meet the requirement of the safety, effectiveness, and quality control standards for clinical application before they can be translated as DDSs. In future, we are interested to design light responsive FONPs for regulated release of neurotransmitters, as FONPs can be easily prepared in the nanorange so that they can effectively release the neurotransmitters in brain cells by removing the blood–brain-barrier. Secondly, we are also interested in developing light responsive FONPs which can release two different neurotransmitters in a sequential or stepwise manner so that we can understand the cross-talk between these neurotransmitters. Third, we also want to construct NIR responsive FONPs for drug delivery applications. Finally, we want to develop agrochemical formulations based on FONPs for the controlled release of sex pheromones and plant growth regulators. Hence, we believe that the above said interesting features of light responsive FONPs will attract several research groups to explore their applications in the fields of biology, medicine, materials chemistry and agriculture in the coming years.

Conflicts of interest

There are no conflicts to declare.

Acknowledgements

We thank the DST SERB (Grant No. EMR/2016/005885 & DIA/2018/000019), and CSIR (Sanction Letter No. 02(367)/19/EMR-II)

for funding. AC is thankful to UGC, New Delhi, and AP and AS are thankful to IIT Kharagpur for financial support.

Notes and references

1 M. S. Yavuz, Y. Cheng, J. Chen, C. M. Cobley, Q. Zhang, M. Rycenga, J. Xie, C. Kim, K. H. Song, A. G. Schwartz, L. V. Wang and Y. Xia, *Nat. Mater.*, 2009, **8**, 935–939.
2 J. R. Heath, M. E. Davis and L. Hood, *Sci. Am.*, 2009, **300**, 44–51.
3 D. Peer, J. M. Karp, S. Hong, O. C. Farokhzad, R. Margalit and R. Langer, *Nat. Nanotechnol.*, 2007, **2**, 751–760.
4 S. Ganta, H. Devalapally, A. Shahiwala and M. Amiji, *J. Controlled Release*, 2008, **126**, 187–204.
5 A. Zhang, K. Jung, A. Li, J. Liu and C. Boyer, *Prog. Polym. Sci.*, 2019, **99**, 101164.
6 S. M. Moghimi, A. C. Hunter and J. C. Murray, *Pharmacol. Rev.*, 2001, **53**, 283–318.
7 S. Xu, Y. Luo and R. Haag, *Macromol. Biosci.*, 2007, **7**, 968–974.
8 S. S. Agasti, A. Chompoosor, C. You, P. Ghosh, C. K. Kim and V. M. Rotello, *J. Am. Chem. Soc.*, 2009, **131**, 5728–5729.
9 S. Angelos, Y. Yang, N. M. Khashab, J. F. Stoddart and J. I. Zink, *J. Am. Chem. Soc.*, 2009, **131**, 11344–11346.
10 Y. Zhu and M. Fujiwara, *Angew. Chem., Int. Ed.*, 2007, **46**, 2241–2244.
11 A. Bansal and Y. Zhang, *Acc. Chem. Res.*, 2014, **47**, 3052–3060.
12 G. S. Kumar and D. C. Neckers, *Chem. Rev.*, 1989, **89**, 1915–1925.
13 C. Park, J. Lim, M. Yun and C. Kim, *Angew. Chem., Int. Ed.*, 2008, **47**, 2959–2963.
14 H. Lin, W. Xiao, S.-Y. Qin, S.-X. Cheng and X.-Z. Zhan, *Polym. Chem.*, 2014, **5**, 4437–4440.
15 Y. A. Lau, B. L. Henderson, J. Lu, F. Tamanoi and J. I. Zink, *Nanoscale*, 2012, **4**, 3482–3489.
16 J. Liu, W. Bu, L. Pan and J. Shi, *Angew. Chem., Int. Ed.*, 2013, **52**, 4375–4379.
17 S. Karthik, A. Jana, B. Saha, K. K. Behera, S. K. Ghosh, Y. Zhao and N. D. Pradeep Singh, *J. Mater. Chem. B*, 2014, **3**, 728–732.
18 S. Karthik, B. Saha, S. K. Ghosh and N. D. Pradeep Singh, *Chem. Commun.*, 2013, **49**, 10471–10473.
19 S. Karthik, N. Puvvada, B. N. P. Kumar, S. Rajput, A. Pathak, M. Mandal and N. D. Pradeep Singh, *ACS Appl. Mater. Interfaces*, 2013, **5**, 5232–5238.
20 Q. Lin, Q. Huang, C. Li, C. Bao, Z. Liu, F. Li and L. Zhu, *J. Am. Chem. Soc.*, 2010, **132**, 10645–10647.
21 S. S. Agasti, A. Chompoosor, C. You, P. Ghosh, C. K. Kim and V. M. Rotello, *J. Am. Chem. Soc.*, 2009, **131**, 5728–5729.
22 J. L. Vivero–Escoto, I. I. Slowing, C. Wu and V. S. Y. Lin, *J. Am. Chem. Soc.*, 2009, **131**, 3462–3463.
23 H. Kasai, H. Oikawa, S. Okada and H. Nakanishi, *Bull. Chem. Soc. Jpn.*, 1998, **71**, 2597–2601.
24 X. Su, J. Zhang, L. Sun, T. W. Koo, S. Chan, N. Sundararajan, M. Yamakawa and A. A. Berlin, *Nano Lett.*, 2005, **5**, 49–54.
25 P. Klan, T. Solomek, C. G. Bochet, A. Blanc, R. Givens, M. Rubina, V. Popik, A. Kostikov and J. Wirz, *Chem. Rev.*, 2013, **113**, 119–191.
26 A. Jana, M. Ikbal and N. D. Pradeep Singh, *Tetrahedron*, 2012, **68**, 1128–1136.
27 A. Jana, B. Saha, M. Ikbal, S. Ghosh and N. D. Pradeep Singh, *Photochem. Photobiol. Sci.*, 2012, **11**, 1558–1566.
28 A. Jana, B. Saha, S. Karthik, S. Barman, M. Ikbal, S. K. Ghosh and N. D. Pradeep Singh, *Photochem. Photobiol. Sci.*, 2013, **12**, 1041–1052.
29 Y. Venkatesh, Y. Rajesh, S. Karthik, A. C. Chetan, M. Mandal, A. Jana and N. D. Pradeep Singh, *J. Org. Chem.*, 2016, **81**, 11168–11175.
30 Y. Venkatesh, H. K. Srivastava, S. Bhattacharya, Mu. Mehra, P. K. Datta, S. Bandyopadhyay and N. D. Pradeep Singh, *Org. Lett.*, 2018, **20**, 2241–2244.
31 A. Chaudhuri, Y. Venkatesh, K. K. Behara and N. D. Pradeep Singh, *Org. Lett.*, 2017, **19**, 1598–1601.
32 A. Paul, A. Biswas, S. Sinha, Sk. S. Shah, M. Bera, M. Mandal and N. D. Pradeep Singh, *Org. Lett.*, 2019, **21**, 2968–2972.
33 A. Paul, R. Mengji, M. Bera, M. Ojha, A. Jana and N. D. Pradeep Singh, *Chem. Commun.*, 2020, **56**, 8412–8415.
34 B. Roy, M. Kundu, A. K. Singh, T. Singh, S. Bhattachary, P. K. Datta, M. Mandal and N. D. Pradeep Singh, *Chem. Commun.*, 2019, **55**, 13140–13143.
35 A. Sikder, M. Banerjee, T. Singha, S. Mondal, P. K. Datta, A. Anoop and N. D. Pradeep Singh, *Org. Lett.*, 2020, **22**, 6998–7002.
36 A. Jana, K. S. P. Devi, T. K. Maiti and N. D. Pradeep Singh, *J. Am. Chem. Soc.*, 2012, **134**, 7656–7659.
37 A. Jana, B. Saha, D. R. Banerjee, S. K. Ghosh, K. T. Nguyen, X. Ma, Q. Qiuyud, Y. Zhao and N. D. Pradeep Singh, *Bioconjugate Chem.*, 2013, **24**, 1828–1839.
38 S. Biswas, J. Das, S. Barman, B. R. Pinninti, T. K. Maiti and N. D. Pradeep Singh, *ACS Appl. Mater. Interfaces*, 2017, **9**, 28180–28184.
39 S. Biswas, R. Mengji, S. Barman, V. Vangala, A. Jana and N. D. Pradeep Singh, *Chem. Commun.*, 2018, **54**, 168–171.
40 S. Barman, S. K. Mukhopadhyay, S. Biswas, S. Nandi, M. Gangopadhyay, S. Dey, A. Anoop and N. D. Pradeep Singh, *Angew. Chem., Int. Ed.*, 2016, **55**, 1–6.
41 T. P. Szatrowski and C. F. Nathan, *Cancer Res.*, 1991, **51**, 794–798.
42 W. Chen, K. Balakrishnan, Y. Kuang, Y. Han, M. Fu, V. Gandhi and X. Peng, *J. Med. Chem.*, 2014, **57**, 4498–4510.
43 H. K. Okur, M. Yuksel, T. Lacin, V. Baysungur and E. Okur, *J. Surg. Oncol.*, 2013, **11**, 9.
44 L. Khandrika, B. Kumar, S. Koul, P. Maroni and H. K. Koul, *Cancer Lett.*, 2009, **282**, 125–136.
45 P. T. Schumacker, *Cancer Cell*, 2006, **10**, 175–176.
46 D. Trachootham, J. Alexandre and P. Huang, *Drug Discovery*, 2009, **8**, 579–591.
47 J. Mei, Y. Hong, J. W. Y. Lam, A. Qin, Y. Tang and B. Z. Tang, *Adv. Mater.*, 2014, **26**, 5429–5479.
48 Y. Hong, J. W. Y. Lam and B. Z. Tang, *Chem. Soc. Rev.*, 2011, **40**, 5361–5388.
49 J. Liang, B. Z. Tang and B. Liu, *Chem. Soc. Rev.*, 2015, **44**, 2798–2811.
50 Z. Zhou, J. Song, L. Nie and X. Chen, *Chem. Soc. Rev.*, 2016, **45**, 6597–6626.
51 C. A. Robertson, D. H. Evans and H. Abrahamse, *J. Photochem. Photobiol., B*, 2009, **96**, 1–8.
52 H. Abrahamse, C. A. Kruger, S. Kadanyo and A. Mishra, *Photomed. Laser Surg.*, 2017, **35**, 581–588.
53 H. C. Huang, S. Barua, G. Sharma, S. K. Dey and K. Rege, *J. Controlled Release*, 2011, **155**, 344–357.
54 J. Yeow, S. Shanmugam, N. Corrigan, R. P. Kuchel, J. Xu and C. Boyer, *Macromolecules*, 2016, **49**, 7277–7285.
55 C. J. Gomer, A. Ferrario, M. Luna, N. Rucker and S. Wong, *Lasers Surg. Med.*, 2016, **38**, 516–521.
56 A. F. Dos Santos, D. R. Q. De Almeida, L. F. Terra, M. S. Baptista and L. Labriola, *J. Cancer Metastasis Treat.*, 2019, **5**, 25.
57 B. Rathore, K. Sunwoo, P. Jangili, J. Kim, J. H. Kim, M. Huang, J. Xiong, A. Sharma, Z. Yang, J. Qu and J. S. Kim, *Biomaterials*, 2019, **211**, 25–47.
58 C. S. Kue, S. Y. Ng, S. H. Voon, A. Kamkaew, L. Y. Chung, L. V. Kiew and H. B. Lee, *Photochem. Photobiol. Sci.*, 2018, **17**, 1691–1708.
59 M. Gangopadhyay, S. K. Mukhopadhyay, S. Gayathri, S. Biswas, S. Barman, S. Dey and N. D. Pradeep Singh, *J. Mater. Chem. B*, 2016, **4**, 1862–1868.
60 D. B. Lovejoy, P. J. Jansson, U. T. Brunk, J. Wong, P. Ponka and D. R. Richardson, *Cancer Res.*, 2011, **71**, 5871–5880.
61 I. Yucel, F. Arpaci, A. Ozet, B. Doner, T. Karayilanoglu, A. Sayar and C. Berk, *Biol. Trace Elem. Res.*, 1994, **40**, 31–38.
62 M. Gangopadhyay, A. Jana, Y. Rajesh, M. Bera, S. Biswas, N. Chowdhury, Y. Zhao, M. Mandal and N. D. Pradeep Singh, *ChemistrySelect*, 2016, **1**, 6523–6531.
63 R. B. Mokhtari, T. S. Homayouni, N. Baluch, E. Morgatskaya, S. Kumar, B. Das and H. Yeger, *Oncotarget*, 2017, **8**, 38022–38043.
64 M. Gangopadhyay, S. K. Mukhopadhyay, S. Karthik, S. Barman and N. D. Pradeep Singh, *MedChemComm*, 2015, **6**, 769–777.
65 A. Chaudhuri, Y. Venkatesh, J. Das, K. K. Behara, S. Mandal, T. K. Maiti and N. D. Pradeep Singh, *ACS Appl. Nano Mater.*, 2018, **1**, 6312–6319.
66 C. Parthiban, M. Pavithra, V. K. Reddy, D. Sen, M. Samuel and N. D. Pradeep Singh, *ACS Appl. Nano Mater.*, 2018, **1**, 6281–6288.
67 C. Parthiban, M. Pavithra, L. V. K. Reddy, D. Sen and N. D. Pradeep Singh, *ACS Appl. Nano Mater.*, 2019, **2**, 3728–3734.
68 A. K. Mustafa, M. M. Gadalla and S. H. Snyder, *Sci. Signaling*, 2009, **2**, re2.
69 L. K. Wareham, H. M. Southam and R. K. Poole, *Biochem. Soc. Trans.*, 2018, **46**, 1107–1118.

70 Y. Venkatesh, J. Das, A. Chaudhuri, A. Karmakar, T. K. Maiti and N. D. Pradeep Singh, *Chem. Commun.*, 2018, **54**, 3106–3109.
71 K. K. Behara, Y. Rajesh, Y. Venkatesh, B. R. Pinninti, M. Mandal and N. D. Pradeep Singh, *Chem. Commun.*, 2017, **53**, 9470–9473.
72 R. Wang, *Physiol. Rev.*, 2012, **92**, 791–896.
73 L. Li, P. Rose and P. K. Moore, *Annu. Rev. Pharmacol. Toxicol.*, 2011, **51**, 169–187.
74 C. Parthiban, M. Pavithra, L. V. K. Reddy, D. Sen, S. M. Samuel and N. D. Pradeep Singh, *Org. Biomol. Chem.*, 2018, **16**, 7903–7909.
75 A. R. Amin, *J. Drug Metab. Toxicol.*, 2012, **S8**, 1–7.
76 K. K. Behara, Y. Rajesh, A. Chaudhuri, M. Gangopadhyay, M. Mandal and N. D. Pradeep Singh, *J. Mater. Chem. B*, 2018, **6**, 6042–6046.
77 J. W. Costerton, P. S. Stewart and E. P. Greenberg, *Science*, 1999, **284**, 1318–1322.
78 L. Hall-Stoodley, J. W. Costerton and P. Stoodley, *Nat. Rev. Microbiol.*, 2004, **2**, 95–108.
79 R. Canaparo, F. Foglietta, F. Giuntini, C. Della Pepa, F. Dosio and L. Serpe, *Molecules*, 2019, **24**, 1991.
80 S. Barman, S. K. Mukhopadhyay, K. K. Behara, S. Dey and N. D. Pradeep Singh, *ACS Appl. Mater. Interfaces*, 2014, **6**, 7045–7054.
81 B. Huang, F. Chen, Y. Shen, K. Qian, Y. Wang, C. Sun, X. Zhao, B. Cui, F. Gao, Z. Zeng and H. Cui, *Nanomaterials*, 2018, **8**, 102.
82 S. Atta, A. Paul, R. Banerjee, M. Bera, M. Ikbal, D. Dhara and N. D. Pradeep Singh, *RSC Adv.*, 2015, **5**, 99968–99975.
83 S. Atta, M. Ikbal, N. Boda, S. S. Gauri and N. D. Pradeep Singh, *Photochem. Photobiol. Sci.*, 2013, **12**, 393–403.
84 S. Atta, M. Bera, T. Chattopadhyay, A. Paul, M. Ikbal, M. K. Maiti and N. D. Pradeep Singh, *RSC Adv.*, 2015, **5**, 86990–86996.